SEPTEMBER 2019 M.Sc. in Civil Engineering ABDIGAFAR OSMAN HEILE

REPUBLIC OF TURKEY

GAZİANTEP UNIVERSITY

GRADUATE SCHOOL OF NATURAL & APPLIED SCIENCES

NUMERICAL ANALYSIS OF FLOW AROUND CYLINDERS

M.Sc. THESIS

IN

CIVIL ENGINEERING

BY

ABDIGAFAR OSMAN HEILE

SEPTEMBER 2019

NUMERICAL ANALYSIS OF FLOW AROUND CYLINDERS

M.Sc. Thesis

in

Civil Engineering

Gaziantep University

Supervisor

Assoc. Prof. Dr. Mehmet İshak YÜCE

by

Abdigafar Osman HEILE

September 2019

REPUBLIC OF TURKEY
GAZİANTEP UNIVERSITY
GRADUATE SCHOOL OF NATURAL & APPLIED SCIENCES
CIVIL ENGINEERING

Name of the Thesis : Numerical Analysis of Flow around Cylinders

Name of the Student : Abdigafar Osman HEILE

Exam Date : 09.09.2019

Approval of the Graduate School of Natural and Applied Sciences

Prof. Dr. A. Necmeddin YAZICI
Director

I certify that this thesis satisfies all the requirements as a thesis for the degree of Master of Science.

Prof. Dr. Hanifi ÇANAKÇI
Head of Department

This is to certify that we have read this thesis and that in our consensus opinion it is fully adequate, in scope and quality, as a thesis for the degree of Master of Science.

Assoc. Prof. Dr. Mehmet İshak YÜCE
Supervisor

Examining Committee Members:	Signature
Assoc. Prof. Dr. Ali AYTEK	…………………..
Prof. Dr. Hanifi ÇANAKÇI	…………………..
Assoc. Prof. Dr. Mehmet İshak YÜCE	…………………..

I hereby declare that all information in this document has been obtained and presented in accordance with academic rules and ethical conduct. I also declare that, as required by these rules and conduct, I have fully cited and referenced all material and results that are not original to this work.

Abdigafar Osman HEILE

ABSTRACT

NUMERICAL ANALYSIS OF FLOW AROUND CYLINDERS

HEILE, Abdigafar Osman
M.Sc. in Civil Engineering
Supervisor: Assoc. Prof. Dr. Mehmet İshak YÜCE
September 2019
67 pages

Fluid flow around bluff bodies such as circular, square and elliptic cylinders are basic problems in fluid mechanics and has gained much interest in the recent years. These cylinders open a way in order to explore compound shape that can hide their external flow effects. Construction engineers model cylinders in some places like offshore structures, bridge piers, tall buildings, etc. Cylinders are an example where the simplicity of fluid is investigated in all three ways analytical, computational and experimental. This thesis discusses the modelling and analyzing of flow around cylinders by utilizing computational fluid dynamics (CFD). A range of Reynolds numbers varying from 2 to $1*10^7$ were employed in analyses to determine the drag coefficient and flow pattern. Simulations of two-dimensional flow around vertical cylinders were carried out by utilizing shear stress transport (SST) k-ω turbulence closure model. The outcomes of this study were compared with the experimental results in the literature.

Key Words: Flow around Circular Cylinder, Flow around Square Cylinder, Flow around Elliptical Cylinder, SST k-ω

ÖZET

SİLİNDİRLER ETRAFINDAKİ AKIMIN SAYISAL ANALİZİ

HEILE, Abdigafar Osman
Yüksek Lisans Tezi, İnşaat Mühendisliği
Danışman: Doç. Dr. Mehmet İshak YÜCE

Eylül 2019
67 sayfa

Dairesel, kare ve eliptik silindirler gibi kaba cisimler etrafındaki sıvı akımı, Akışkanlar Mekaniği'ndeki temel problemlerdendir ve son yıllarda büyük ilgi görmüştür. Sabit şekilli silindirlerin etrafındaki akım alanının çalışılması daha kopleks şekilli yapıların etrafındaki akım alanının anlaşşlması için yol gösterici olurlar. İnşaat mühendisleri, açık deniz yapıları, köprü iskeleleri, yüksek binalar gibi bazı yapıları silindir şeklinde modellerler. Bazı yapıların etrafındaki akım alanını anlamak için silindirlerin etrafındaki akımın analitik, sayısal ve deneysel yöntemler ile araştırılması yaygındır. Bu tezde, hesaplamalı akışkanlar dinamiği (HAD) kullanılarak silindirler etrafındaki akımın modellenmesi ve analizi tartışmaktadır. Sürüklenme katsayısını ve akım alanını belirlemek için analizlerde 2 ila $1*10^7$ arasında değişen Reynolds sayıları kullanılmıştır. Dikey silindirlerin etrafındaki iki boyutlu akım simülasyonları, SST k-ω türbülans modeli kullanılarak gerçekleştirilmiştir. Bu çalışmanın sonuçları literatürdeki deneysel sonuçlarla karşılaştırılmıştır.

Anahtar Kelimeler: Dairesel Silindir Etrafındaki Akım, Kare Silindir Etrafındaki Akım, Eliptik Silindir Etrafındaki Akım, SST k-ω

"Dedicated to my family"

ACKNOWLEDGEMENTS

First and Foremost, praise is to ALLAH, the Almighty, the greatest of all, on whom ultimately we all depend on for sustenance and guidance. I would like to thank Almighty Allah for giving me the opportunity, determination and strength to do my thesis. His continuous grace and mercy was with me throughout my life and ever more during the tenure of my thesis.

I would like to thank my supervisor, Assoc. Prof. Dr. Mehmet İshak YÜCE for his guidance and support throughout the study. I am thankful for his encouragement and motivation.

I would like to express my love and gratitude to my mom and my father for their support, always best wishes.

TABLE OF CONTENTS

LIST OF TABLES

Page

LIST OF FIGURES

Page

LIST OF SYMBOLS

A	Area (m^2)
D	Diameter of the cylinder (m)
F	Force (N)
f	Force per unit volume (N/m^3)
k	Kinetic energy (J)
m	Mass flow rate (kg/s)
W	Width (m)
V	Velocities (m/s)
p	Pressure (N/m^2)
Re	Reynolds number
L1	Upstream length (m)
L2	Downstream length (m)
St	Strouhal number
fs	Shedding frequency of vortices
$\mathbf{C_D}$	Drag coefficient
$\mathbf{F_D}$	Drag force
$\mathbf{P_0}$	Free stream static pressure
$\mathbf{C_P}$	Pressure coefficient
ρ	Density (kg/m^3)
μ	Dynamic viscosity (kg/m s)
ε	Dissipation rate (J/m)
ω	Specific dissipation rate
υ	Kinematic viscosity
a	Acceleration
T	(deviator) stress tensor
∇	Stands for the del-operator
θ	Angle of İncidence
CFD	Computational Fluid Dynamics

DES	Detached Eddy Simulation
DNS	Direct Numerical Simulation
HOC	Higher Order Compact
K	Shear rate
LB	Lattice Boltzmann
LES	Large Eddy Simulation
NS	Navier-Stocks
RANS	Reynolds Averaged Navier-Stoke
RKE	Realizable K- Epsilon
RNG	Renormalization Group
SİMPLE	Semi-Implicit Method For Pressure-Linked Equation
SKE	Standard K-Epsilon
SKO	Standard K-Omega
SST	Shear Stress Transport
TrW	Wake transition
TrSL	Shear layer transition
TrBL	Boundary layer transition
URANS	Unsteady Reynolds A Navier-Stocks
VOF	Volume of Fluid

CHAPTER I

INTRODUCTION

1.1 General

Flow around cylinders has been a subject matter of experimental and numerical analyses for decades in engineering application. The areas that engineers widely use are offshore structures, bridge piers, power lines, etc. The flow around cylinders shows several significant cases, such as flow separation, turbulence and vortex shedding. Vortex shedding is swinging flow which happens when a fluid like air or water past a bluff body at a certain velocity which relays on the shape and the size of the body. The flow around cylinders normally produces forces like drag force, lift force and pressure coefficient. The force in which a flowing fluid applies on a body towards the direction of the flow is known as drag force, and this force is partially dependent on the fluids viscosity. To understand the difference between laminar and turbulent flows around cylinders, many inventive and sophisticated approaches have been suggested. Computational Fluid Dynamics (CFD) which is the tool I used throughout the simulations is convenient tool to show the flow in terms of streamlines, contours lines, velocity vectors, velocity profiles, etc. The simplest way to define drag coefficient, pressure coefficient and the forces produces on the body is by using CFD techniques. The shear stress transport (SST) k-ω turbulence model was used throughout the simulations.

1.2 Aim of Study

The main purpose of this thesis is to understand the impact of the viscous flow past circular, square (or rectangle) and elliptic cylinders, and to check which shape will give the best result by comparing with the previous experiments. The simulation analyses were tested by performing shear stress transport (SST) k-w turbulence closure model, with Reynolds number varies from 2 to 10^7. The drag coefficients for the circular, square and elliptic cylinders are clarified and made comparison with the experimental results in the literature.

1.3 Outline of the Thesis

General information and the introduction about flow around cylinders, and the objective of the study are detailed in Chapter 1. Flow around bluff bodies, regimes of flow, vortex shedding, vortex-shedding frequency, forces acting on the cylinder, drag force, pressure distribution, effects of the cross-sectional shape on drag coefficient, flow around square cylinder, flow around circular cylinder and flow around elliptical cylinder are explained in Chapter 2.

Governing equations such as momentum, continuity and Navier-stoke equations, an outline of computational fluid dynamics, CFD simulation process, pre-processor, solver and post-processor, turbulence, CFD turbulence model, k-w turbulence model, SST k-w model, standard k-w model, simulation and modeling procedure, geometry and boundary condition, meshing, solving the model and initialization are detailed in Chapter 3

In Chapter 4 results of the simulation of flow around circular, square and elliptical cylinders, velocity streamlines, velocity contours, velocity profiles, drag coefficient, comparison of velocity streamlines of flow around circular, square and elliptical cylinders at certain Reynolds number are explained well. The conclusion of the thesis is summarized in Chapter 5.

CHAPTER 2

FLOW AROUND BLUFF BODIES

2.1 Introduction

The wake flow around cylinders was discovered in the first half of 20th century. There are many experimental and computational investigations in the literature review, which analyzed the flow around bluff bodies at various Reynolds number.

This thesis focuses exclusively on the flow around circular, square and elliptic cylinders. An easy geometry of a bluff body exerts complicated flow phenomena that strongly depends on the Re. The flow behind the cylinders has an unstable wake (vortex shedding), turbulent translation in various regimes of flow as a function of Re, and oscillating points of separation and stagnation. One of the most difficult features of the cylinder flow is the dominant dependence of many local characteristics of flow on Reynolds number. CFD codes have been widely used by many investigators in order to test square, circular and elliptic cylindrical models under different flow conditions.

2.2 Regimes of Flow

The non–dimensional parameters defining the flow around cylinders depend on the Reynolds number (Re) given by:

$$Re = \frac{\text{Inertial force}}{\text{Viscous force}} = \frac{VD}{\upsilon} = \frac{\rho VD}{\mu} \quad (2.1)$$

Where V (m/s) is the flow velocity, D (m) is the diameter of the cylinder, υ is the kinematic viscosity, μ (kg/m. s) is the dynamic viscosity and ρ (kg/m^3) is density. The flow faced huge change as Reynolds number increased from zero. Increasing Reynolds numbers will lead to form an unsteady flow in the wake region of the cylinders, named vortices. Table 2.1 demonstrates the regimes of flow around circular cylinder and the formation of wake region for different Reynolds numbers in steady current.

Table 2.1 Flow regimes around circular cylinder in steady current (Sumer B.M. and Fredsøe J. 2006)

	Non- separation Flow is creep	Re less than 5 (Re < 5)
	Steady separation A steady couple of uniform vortices	40 > Re > 5
	(periodic) vortex street is laminar	200 > Re > 40
	Change to turbulence within the wake	300 > Re > 200
	Wake is fully turbulent. A. separation of the boundary layer is laminar	3×10^5 > Re > 300 Sub-critical
	A. Separation of the boundary layer is laminar. B. Turbulent at boundary layer separation : but laminar at the boundary layer	3.5×10^5 > Re > 3×10^5 Critical
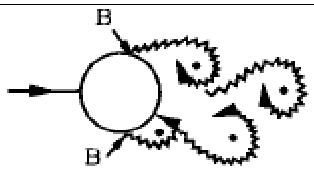	B. Separation of the boundary layer is turbulent, also boundary layer partially laminar partially turbulent.	1.5×10^6 > Re > 3.5×10^5 Supercritical
	C. Entirely turbulent at one phase in boundary layer.	4×10^6 > Re >1.5×10^6 Upper-transition
	C. Two sides in the boundary layer are entirely tuebulent.	Re > 4×10^6 Trans critical

A "bluff body" can possess sharp edges on its boundary, such as a flat plate normal to the flow, rounded edges like circular cylinders. Regardless of the shape, the flows around bluff bodies share common features.

The flow around circular cylinders is distinguished by change of local velocity in terms of the magnitude and direction in time compared to the free stream velocity (AlRefaei, 2009). Figure 2.1 shows the flow regions around circular cylinder. Alrefaie (2009) describes the development of transition from laminar to turbulent in many areas behind the flow around cylinders at different Reynolds numbers: (a) transition in wakes (TrW); (b) and (c) transition in shear layers (TrSL); and (d) transition in boundary layers (TrBL) (Figure 2.2).

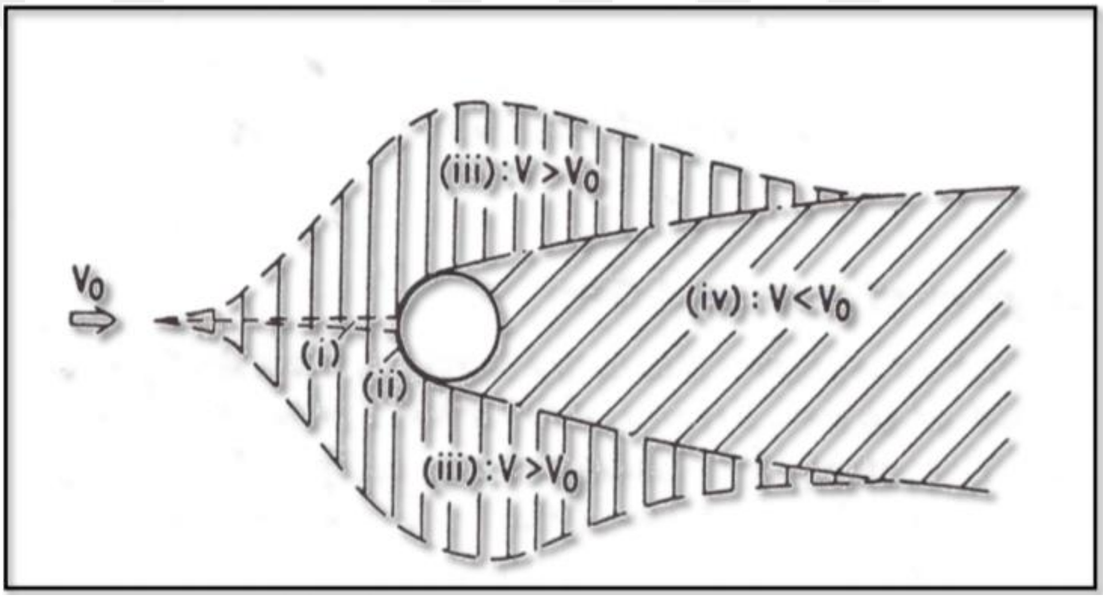

Figure 2.1 Regions of unstable flow (i) One thin area of decelerating flow, (ii) Two boundary layers connected to the surface of the cylinder, (iii) Two oblique areas of repositioned and sped up flow, (iv) One broad region downstream of the parted flow called the wake (Alrefaie, 2009)

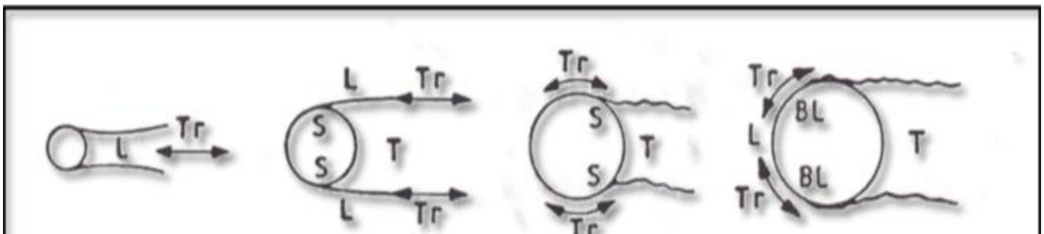

Figure 2.2 Transitions of the flow behind a circular cylinder (a) TrW (b), (c) TrSL (d) TrBL (Alrefaie, 2009)

The dominant parameters in the fluid flow around cylinders are the impact of Reynolds number. For little values of Re < 0.2 no separation happens. Viscous forces control on separation around the surface of the circular cylinder in such a way that all interrupted regions remain laminar. The creeping flow around a cylinder maintains without separation up to Re≈5. Attached couple of vortices structure form within the wake behind the cylinder for 5 < Re < 40, the vortices length development rise with expending Re. At the point when Re is over expended, the wake ends up unsteady which at last bring the vortex shedding phenomena. Vortex is shed in turns at the two sides of the cylinder at a definite frequency. In this manner, the wake has the parts of the vortex street (Kareem, 2015).

For the scope of the Reynolds number expanding from 40-200, laminar vortex street takes place. The shedding is crucially 2D, it doesn't alter the span wise direction. As the Re increased in the rate 200 < Re < 300, the area of transition to turbulence moves away from the obstacle. Sumer and Fredsøe (2006) study that the vortices formed are turbulent at Re =400. The 2D character of the shedding vortex found for the range of 40 < Re < 200, become obviously 3D in this scope. It may be mentioned that the vortex shedding characteristic succeeds for the rest Reynolds number regimes Re > 300 (Kareem, 2015).

The wake entirely turbulent for Reynolds number greater than 300 (Re > 300). The boundary layer stays laminar when the Re number are widely increasing 3×10^5 > Re > 300, for this state the regime is called subcritical regime of flow. Conversion to turbulence in the boundary layer takes place as the Re keeps enlarging. The conversion state at the earliest occurs at the point of the border layer parts, when Re increase the transition region to the turbulence goes upstream on the top of the cylinder towards the point of stagnation. In the narrow Re band of $3 \times 10^5 < Re < 3.5 \times 10^5$ as shown in Table2.1, the boundary layer will be turbulent at the point of separation, regardless of this taking place just for one of the phases of the cylinder. Consequently, boundary layer separation is turbulent at one phase of the surface cylinder and the opposite side is laminar. This regime is known as critical. As illustrated in Table 2.1 as the Re increases between 35×10^4 and 15×10^5, this is known as supercritical flow regime. The boundary layer separation is turbulent in this regime on either sides of the cylinder. Nevertheless, progress in the boundary layers of the turbulence hasn't been performed at this point. Transition to turbulent area found somewhere close to the separation and stagnation points. When Re range 1.5 x 10^6 on one side of the boundary layer becomes completely turbulent and the opposite side of the cylinder is partially turbulent. This kind of regime is said to be upper- transition flow of the regime, which dominates over the range of 4.5x10^6>Re>1.5 x 10^6. For Re ranges 45 x 10^5 the boundary layer on the top of the cylinder called the trans-critical flow regime which is effectively turbulent everywhere.

2.3 Vortex Shedding

The notion of vortex shedding was established in (Sumer and Fredsoe, 1997). Given that Re > 40 the boundary layer on the top of the cylinder separates because of the disadvantageous pressure gradient. This pressure gradient emerges due to the dissimilar environment of the flow at the back of the cylinder. Consequently, a shear layer is formed. The boundary layer alongside the cylinder constitutes of notable number of vortices. The vorticity continues into the shear layer at the downstream of the separation point and lead the shear layer to form into a vortex with a sign same as that of moving toward vortices (Figure 2.3).

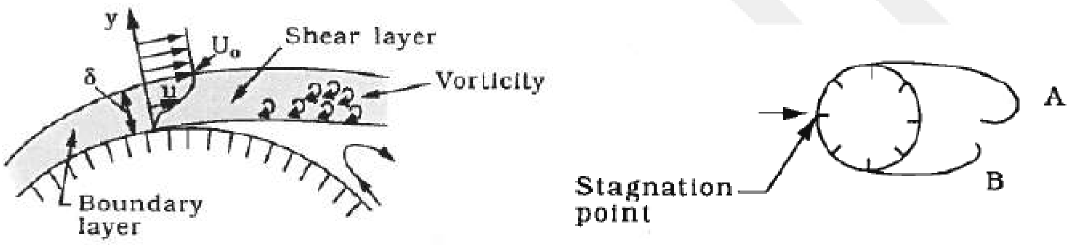

(a) Flow nearby separation (b) Starting of the vortex shedding

Figure 2.3 The boundary layer, the shear layer downstream of the cylinder and the starting of the vortex shedding is shown, from (Sumer and Fredsoe ,1997).

2.3.1 Vortex-Shedding Frequency

The notion of shedding the vortex is established in Sumer and Fredsoe (1997). The coefficient of the lift was developed by Establishing Strouhal number St, shedding of the vortex period from the plot T_v. Developments can be done from the swinging pressure to examine in the wake next to the cylinder.

Whereby vortex shedding frequency, f_v is given by:

$$f_v = \frac{1}{T_v} \tag{2.2}$$

Normalization of the vortex shedding frequency is also possible by the use of flow velocity U_c combined with the cylindrical diameter D. This is called strouhal number (S_t) this can be computed by this formula:

$$S_t = S_t\,(Re) \quad (2.3)$$

in which

$$S_t = \frac{f_v D}{U_c} \quad (2.4)$$

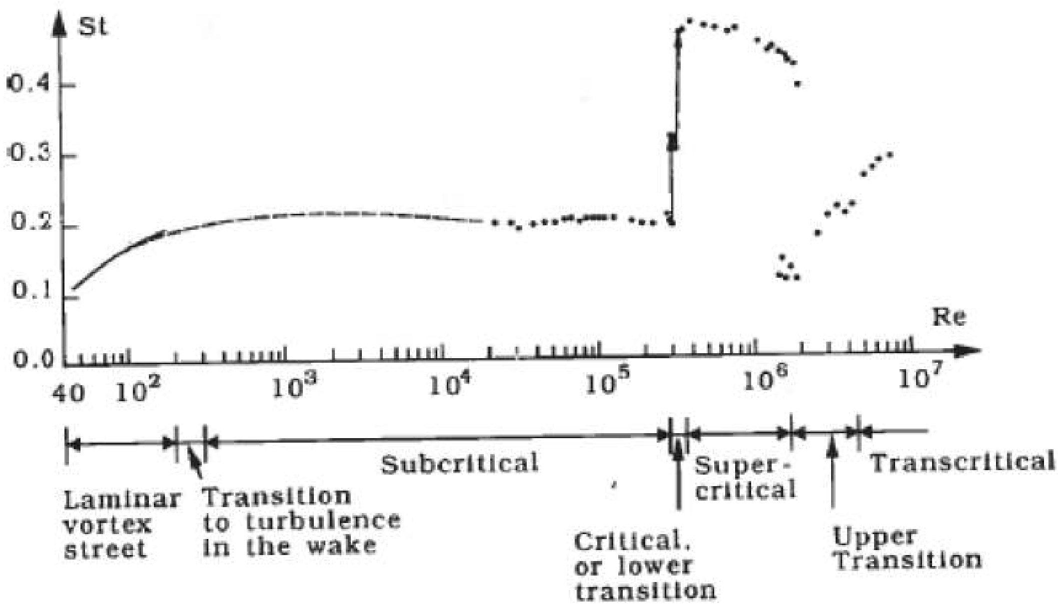

Figure 2.4 Strouhal number for circular cylinder with respect to Reynolds number (Sumer and Fredsoe, 1997).

2.4 Forces Acting on a Cylinder

This notion is created through (Sumer and Fredsoe, 1997). A resultant power will exert on a cylinder. The two inputs to this force are: one comes in the form of pressure and the other comes in the form of friction. The sum total in-line power is known as mean drag, which is the sum of the total in-line mean pressure force and the in-line mean friction force. When Re > 40, as a result of the fixed interval vortex shedding, the pressure will also have fixed interval change, thus also the force elements will have a fixed interval variation. The drag force changes periodically with time and is rotating around a mean value; the mean drag. Another power is rotating lift force, which also have fixed interval changing. Nevertheless, this power has a mean value which equates to zero due to the symmetry of the flow. Figure 2.5 shows how the lift and drag forces change with time.

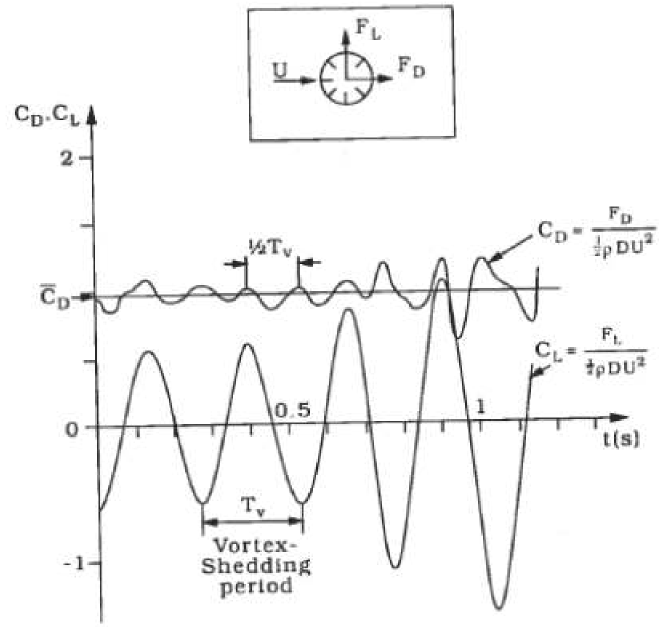

Figure 2.5 drag and lift forces coefficients obtained from the measure of Pressure distribution, created in (Sumer and Fredsoe ,1997).

2.4.1 Drag Force

The phenomenon of fluid flow over a solid object can be simulated and measured by the drag coefficient. Drag force (friction drag) one of the main forces which is applied by fluid flows on the surface of solid obstructions, in the reverse direction of the relative flow velocity. The drag force applied on an object by a fluid depends on several factors including the physical properties of the fluid, the shape and the size of the solid object and the velocity of the fluid (or the solid object). These factors make it hard to accurately calculate the drag force applied on a body. The development of eddies and the alternating vortex shedding phenomena, which appears in the wake of the cylinder, cause an irregular and non-uniform pressures distribution. This disparate distribution of pressure also contributes to the drag force.

The drag coefficient is usually designated as C_D; the C_D is a non-dimensional quantity which can be used to describe the drag or the resistance of an obstacle in a fluid movement. The lesser drag coefficient shows the object has less amount of hydrodynamic or aerodynamic drag and vice versa. The C_D is always related to a specific surface area. The drag coefficient can be changeable under different flow conditions. The value of drag coefficient changes with Reynolds number, orientation, shape, velocity, flow direction, objects position, density, object size and viscosity of fluid (Yuce and Kareem, 2016).

Two techniques are in charge of drag, inertial forces and viscous forces. Broadly, the inertial forces increase when a fluid imports its lost momentum into an object. However, the viscous forces begin from the sheared flow of fluid around the obstacle. The viscous component of the drag form because of the shear stress. One of the two inertial forces and the viscous forces are predicted to be the major contributors to the drag, which is depending on the size of the object and strength of the flow. Generally, the inertia to viscous forces is defined as a Reynolds number.

Equation 2.5 illustrated the core relationship between the drag coefficient on a solid body and the drag force.

$$C_D = \frac{2F_D}{\rho V^2 A} \qquad (2.5)$$

where F_D is the drag force, ρ is the density of the fluid, V is the velocity of the fluid relative to the particle, the C_D is the drag coefficient of any particle and A is the reference area. Two different methods can be used to find the drag coefficient. The obvious way to compute the C_D as in equation 2.5 which directly measures the F_D and the velocity of the flow V. The other technique to discover F_D is by using the moody chart with C_D against Re for well-known object shapes. Figure 2.6 illustrates the difference in C_D against Re.

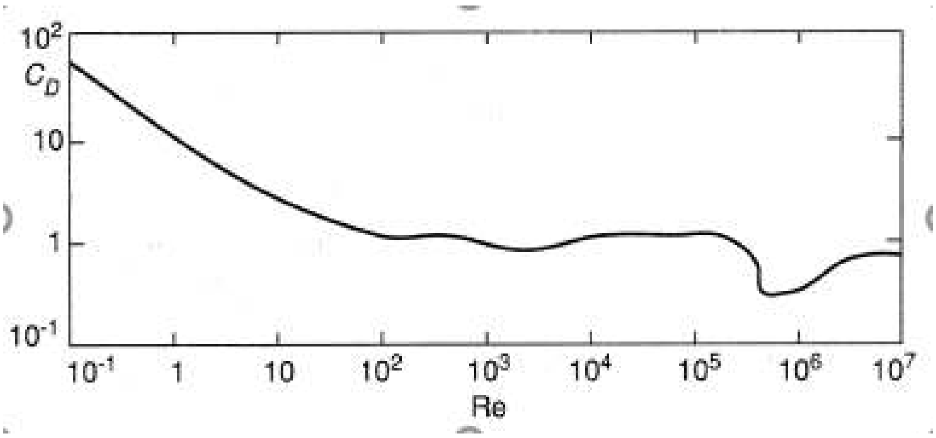

Figure 2.6 Drag Coefficient-Reynolds number of the circular cylinder (Hoerner, 1965)

2.4.2 Pressure Distribution

Pressure distribution is the main part of total drag force which due to the pressure applied around an object when fluid flows. According to Cattolica, (2003). The drag coefficient can be calculated by the pressure distribution method, by putting on record the value of the surface pressure, static pressure, total pressure & pressure coefficient as well.

$$C_p = \frac{2(p\text{-}Po)}{\rho U^2} \tag{2.6}$$

Where C_p is coefficient of the pressure, p is surface pressure, Po is free stream static pressure

ρ is fluid density and U fluid flow velocity.

Then

$$C_D = \int_0^{2\pi} C_p \cos\theta \tag{2.7}$$

2.5 Effects of Cross-Sectional Shape on Drag Coefficient

As the velocity of flow increases some factors are expected to decrease in the drag coefficient, while some factors might cause to increase in the drag coefficient when flow velocity decreases. It should be noted that drag coefficient (CD) doesn't have constant number on each shape. It changes mainly with Reynolds number and velocity of flow as well. Here are some of the factors which impact the drag coefficient out of the flow around cylinder (Kareem, 2015);

1. The size of the obstacle and the shape; the cross-sectional shape and the roughness of the surface of the object have an impact on the drag coefficient, a smooth surface has less drag coefficient when it compares to roughness one. The surface roughness and cross-sectional shape have direct impact on the drag coefficient. Table 2.2 indicates the effect of the cross-sectional shapes on the drag in 2D.
2. The velocity of the flow, the mass flow rate and the viscosity of the fluid; whereby the drag force actually changes with the square of the relative velocity linking the object to the fluid. The tendency of the body corresponds to the direction of the flow which is also expected to affect the quantity of drag produced by an object. Drag coefficient relies on the mass of the flow flowing past an object. Also, the

drag coefficient is depending on a composite way on two things of the liquid, which are viscosity and its compressibility.

Table 2.2 The impact of the cross-sectional shape on the drag coefficient in two dimensional 2D for Re > 10^4 (Noor, 2015).

No.	Body	Status	Shape	C_d
1	Square rod	Sharp corner		2.2
		Round corner		1.2
2	Circular rod	Laminar flow		0.3
		Turbulent flow		1.2
3	Equilateral triangular rod	Sharp edge face		1.5
		Flat face		2
4	Rectangular rod	Sharp corner	L/D = 0.1	1.9
			L/D = 0.5	2.5
			L/D = 3	1.3
		Round front edge	L/D = 0.5	1.2
			L/D = 1	0.9
			L/D = 4	0.7
5	Elliptical rod	Laminar flow	L/D = 2	0.6
			L/D = 8	0.25
		Laminar flow	L/D = 2	0.2
			L/D = 8	0.1
6	Symmetrical shell	Concave face		2.3
		Convex face		1.2
7	Semicircular rod	Concave face		1.2
		Flat face		1.7

2.6 Flow Around Circular Cylinder

Flow past a circular cylinder is one of the most significant concepts of mechanics. The areas that can be applied on the flow around bluff bodies are offshore, marine engineering and marine pipelines. It can also be applied in construction applications like long-span bridges, flow around chimney stacks, tall buildings, transport ships, heat exchanger, towers, etc. For structural damage to be avoided it's important to lower vortex-induced vibrations, lift and drag forces acting on them. Thus, it's important to adjust a new technique regarding flow around a circular cylinder in order to lower structural damage and enhance the shelf life of the cylinder which is used for particular application.

Kanaris et al. (2011) studied direct numerical simulations of two and three dimensions of the flow around circular cylinder positioned uniformly in a plane channel. Reynolds number with a range of 10-390 which has a blocking ratio of 0.2 was used. Results show that the flow will remain 2D for the Reynolds number up to Re=180. For greater values of the Reynolds number, re $\geq$210 the effect of 3D flow evolves and and drag, CD, time history of lift, CL, coefficients were illustrated. Catalano et al. (2003) investigated Large Eddy Simulation (LES) which has a wall modeling for higher Reynolds number range of $5*10^5$ to 10^6 in the supercritical regime is carried out by evaluating flow around a circular cylinder. The estimated boundary condition to the LES can be obtained by the use of Wall stress model. Results are put in comparison with those of the experimental data and unsteady Reynolds-average Naiver-stoke solutions (RANS). LES results showed to be rather much precise compare to RANS results. Ong et al. (2010) simulated two-dimensional (2D) flow around a circular cylinder with high Reynolds number near a flat seabed. k–ε turbulence closure model was utilized, also the impact of the flat seabed roughness, Reynolds number and gap to diameter ratio for a particular border layer thickness of inlet flow of the cylinder has been carried out. Zhao and Lu (2018) applied direct numerical simulations for Reynolds numbers ranging from 100 to 500 of flow around two circular cylinders in a cruciform order. The reason behind this study is to control the regional flow pattern nearby the gap between the two cylinders, the impact of the force coefficient of the two cylinders and the round vortex shedding flow of the cylinders. The three specified regional flow patterns nearby the gap are: necklace vortex (NV), trial vortex (TV) and the vortex shedding in the gap (SG) which comply with those in the experimental data.

Islam and Raghavan (2006) studied unsteady 2D flow around circular cylinder in a confined duct with suitable blockage ratio. In this numerical solution Reynolds number ranges from 200-100000 are investigated. The results agree considerably well with the experiment both in the drag coefficient and pressure distribution. Cao and Tamura (2009) used LES and DNA to see the shear influence on flow around circular cylinder at Reynolds number ranging from 60-1000. Investigations are carried out to determine the difference of strouhal number, lift coefficients, drag coefficients and unstable wake structures with shear parameter and their Reynolds number.

Ong et al. (2009) studied high Reynolds number flow ($1*10^6$, $2*10^6$, $3.6*10^6$) covering the subcritical to upper-transition flow regimes around 2D smooth circular cylinder have been carried out numerically by using 2D Unsteady Reynolds-Averaged Navier–Stokes(URANS) equations with a standard high Reynolds number k-ε turbulence model. The objective of the study is to evaluate whether the model is applicable for engineering design within these flow regimes. The results are complied well with experimental data and numerical results.

Hamielec and Raal (1969) studied numerical simulations for incompressible newtonian flow around circular cylinder with Reynolds number of 1, 2, 4, 10, 15, 30, 50, 100 and 500. The results are made in the form of stream function distribution and vorticity. The solutions give detailed charectirization of the drag coefficient, vortex rings, pressure distribution and vortex dimensions are compared with theoretical solutions and experimental data for reynolds number up to 50. The solution agreed well with the experimental data and prior theoretical solutions.

Zhang et al. (2014) applied standard k–ε model in the subcritical to supercritical offshore flow regimes via resembling flow past a circular cylinder at Re= 10^5, $5*10^5$ and 10^6. To analyze the convergence of the k–ε turbulence model, a number of meshes with Various grid and time step size resolutions are picked for every Reynolds number. Mehdi et al. (2016) carried out flow around 2D circular cylinder with low Reynolds number of 200, 500 and 1000 with the various angle of attack 0°,5° and 10°. Complete Pressure fine volume method and the second-order complete scheme is used in this simulation. İn this flow Navier-stoke and continuity equation has been investigated. The drag coefficient, the pressure, and vortex shedding for various Reynolds numbers with the different angle of attack were counted up and matched with other numerical results which have shown good agreement.

Benim et al. (2007) used RANS formulation for study of turbulent flow around a circular cylinder. There are difficulties in using wall function method for designing the near wall turbulence which was discussed. Reynolds number ranges from 10^4 to $5*10^6$ covering the critical regime is investigated. SST model is utilized to fix the near wall layer. Rajani et al. (2012) simulated two-dimensional flow around a circular cylinder with Reynolds number ranging from 10^4-10^7 by the use of unstable RANS code RANS3D combined to four-eddy viscosity based on the model of the turbulence. For Re= 10^5 in the subcritical region, rational flow patterns with turbulence vortex shedding at (Strouhal number) for specific Reynolds number are predicted by the use of the four turbulence models.

2.7 Flow Around Rectangular Cylinders

Flow around rectangular (square) cylinder is used for several engineering applications, pipelines, bridge piers, tall buildings, chimneys, etc. In this kind of studies two-dimensional and three-dimensional experimental and numerical simulations were carried out to give much understanding of the fundamental flow behaviors (flow patterns) around the structures.

Flow around rectangular cylinders with side ratio of 0.4 and 8 have been computed by using finite different method in the scope of Reynolds number of 100 to $1.2*10^3$, to obtain a better insight into the detailed charecteristics of flows (Okajima et al., 1990).

Yen and Yang (2011) studied flow around and behind square cylinder at different Reynolds number ranging 4000-36000 and incident angles of $0^{\circ}<\theta<45$. With the use of the smoke-wire scheme the flow patterns around and behind square cylinders were specified. The field of velocity were defined by using particle image velocimetry.

Numerical simulations of 2D incompressible linear shear flow around square cylinder were acquired (Cheng et al., 2007). These analyses were done by the use of the lattice Boltzmann method. Reynolds number with ranges $50 \leq Re \leq 200$ and $0 \leq K \leq 0.5$, in which Re and K are Reynolds number and shear rate, in that order. The shear rate impact on frequency of the vortex shedding from the cylinder drag and lift forces applied on the cylinder have been qualified at the same instant with the flow patterns past the cylinder. The outcomes shown indicate that the vortex development at the back of the cylinder is highly dependent on Re and K.

The heat transfers and the flow structure of an isolated square cylinder in cross flow are performed numerically for both stable and unstable recurrent laminar flow in 2D flow regime (Sharma and Eswaran, 2010). Reynolds number of range of 1-160 and a Prandtl number of 0.7 were investigated. Cao and Tamura (2016) simulated flow over square cylinder at Reynolds number of $2.2*10^4$ using large-eddy simulation with fine mesh which have a cell number over 7 million. The precision of LES on structured and un-structured grids is evaluated from engineering point of view, and compared with preceding studies. Kumara and Raya (2015) investigated two-dimensional incompressible shear flow around square cylinder. These simulations were done using the newly established higher order compact (HOC) scheme. Reynolds number and shear rate ranges of 100 to 200 and 0.0 to 0.1, respectively were used.

Yuce and Kareem (2016) investigated the two-dimensional flow around cylinders with same characteristic length scale under the same flow states. In this study Reynolds number ranging from 2 to $4*10^6$ were carried out by employing shear stress transport closure model.

2.8 Flow Around Elliptic Cylinder

High Reynolds number flows including the super-critical the upper- transition regimes of flow through a two-dimensional (2D) elliptical cylinder having performed numerically by the use of 2D (URANS) equations. Reynolds numbers used in the study were ($0.5*10^6$, $1*10^6$, $2*10^6$, $3.6*10^6$). The aim of the analyses is to assess the drag coefficient through the outer surface of elliptical cylinder with minor-to-major axis ratio of 0.4, 0.6, 0.8 for different types of velocity input (Rawat et al., 2013). Kim and Sengupt (2005) studied the unsteady viscous flow physics over two-dimensional ellipse using SIMPLER method in the intrinsic curvilinear coordinate system by computing the two-dimensional Navier stokes equation. Unstable viscous flows over different thickness to chord ratios of 0.6, 0.8, 10 and 12 elliptical cylinders are analyzed with various Reynolds number of 200, 400, 1000. The reason behind this study is to understand the effect that elliptic cylinder thickness and Reynolds number have on the lift and drag forces.

Taeibi-Rahni et al. (2013) investigated laminar flow around elliptic cylinder confined in a channel. The lattice Boltzmann method is utilized to simulate flow in two-dimensions. The simulations are performed in a range of condition, $5 \leq R \leq 100$, (Reynolds number), $0 \leq \theta \leq 90$, (angle of incidence) and for AR= 0.25, 0.5, (aspect ratio). In this study, the impact of aspect ratio on steady laminar flow around an elliptical cylinder is carried out numerically at low Reynolds number 20 and 40 (Didier, 2009). The two-dimensional Navier-stokes equations are computed by using an original fully coupled resolution method.

Mostafa et al. (2014) performed an exploratory analysis to explain the characteristics of flow of heat transfer through an elliptic cylinder. Furthermore, the envisioning of the flow was done to explain the flow designs through the cylinder. The elliptic cylinder which has an axis ratio of 1:2.17, was situated toward the parabolic plate. The test flow is air and Reynolds number ranges from $5*10^3$ to $3*10^4$.

Flow around elliptic cylinders were examined for various Reynolds numbers and angles of attack in two-dimensional unstable incompressible Navier-stokes equations that can be solved numerically (Nair and Sengupta, 1997).

CHAPTER 3

METHODOLOGY

3.1 Governing Equation

Energy equation, continuity equation and navier-stokes (N-S) are used like governing equations for two-dimensional (2D) turbulent incompressible flow around cylinders. The fluid should be homogeneous structure.

3.1.1 Energy Equation

Energy equation is the first law of thermodynamics, which states that the rate of change of energy inside the fluid element is proportionate to the net flux of heat into the element plus the rate of working done on the element as a result of the body and surface forces.

3.1.2 Navier-Stokes Equation

This equation was created by Claude-Louis Navier and George Stokes, which describes the viscous fluids, the equation is used for Newton's second law of motion.

$$\Sigma F = ma \tag{3.1}$$

The left-hand side is the sum total of outer forces pressure, stress and internal body forces. While the inertia is on the right-hand side. The acceleration of particle at a point is defined as viscous fluid of the substance.

$$a = \frac{DV}{DT} \tag{3.2}$$

The Navier Stokes equations were determined using Newton's second law which is based on conservation of momentum that is written for a random quantity of the fluid in an inertial frame of reference, the formulation of Navier stoke equation is:

$$\rho\left(\frac{\partial V}{\partial t} + V.\nabla \mathrm{V}\right) = -\nabla P + \nabla.\mathrm{T} + \mathrm{f} \tag{3.3}$$

Where v is the flow velocity, ρ is the fluid density, P is the pressure, T is the (deviator) stress tensor, f represents body forces (per unit volume) acting on the fluid and ∇ represents del-operator.

3.1.3 Continuity Equation

The derivation of continuity equation comes from the principle of conservation of mass. The continuity equation indicates that the rate at which mass enters a body is said to be equal to the rate at which mass leaves a body plus the accommodation of mass in the system. This condition is only valid for steady flows. For incompressible flow the continuity equation is like this:

$$\frac{\partial u_i}{\partial x_i} \tag{3.4}$$

3.1.4 Momentum Equation

Applications of Newton's second law drives the momentum equation and relates the sum total of the forces acting on the element of fluid to its acceleration or rate of change of momentum. Newton's second which states that the rate of change of momentum of a body is equivalent to the resulting force acting on the body, which occurs in the direction of the force. The momentum equation is written as follows:

$$\frac{\partial u_i}{\partial t} + \frac{\partial u j u_i}{\partial x_j} = \frac{\partial}{\partial x_j}\left(\mu \frac{\partial u_i}{\partial x_j}\right) - \frac{1}{\rho}\frac{\partial p}{\partial x_i} \tag{3.5}$$

3.2 Outline of Computational Fluid Dynamics

Computational Fluid Dynamics (CFD) is a section of fluid mechanics which deals with the prediction of mass, heat and momentum transfer and optimal design in the industrial process. It's also used to utilize the numerical method and turbulence closure models that allow to investigate how the dynamic fluid flow works. CFD utilizes applied mathematics and powerful computers to model fluid flow situations. It's easy to create a computational model of the system or device that we want to examine by using Computational Fluid Dynamics. Physics of fluid flow is applied in addition to software and some chemistry which produce the fluid dynamics that associates with physical phenomena. The development of CFD has gained very wide attention whole to the international community since the advent of digital computer. CFD is capable of simulating the flow of liquid, gases, multiphase physics, chemical reaction, fluid-structure interaction and acoustics via computer modeling heat and mass transfer moving bodies. Using computers, CFD nowadays becomes an essential member of analyses and engineering design. Engineers are capable of making good use of CFD tools for simulation of the flow of the fluid and heat transfers that a system model can project the performance of the system prior to producing it.

Users utilize CFD techniques in a wide range of industrial application areas like: mechanical works, refrigeration and air conditioning system, combustion system in gas turbines and engines, transmission system in gas and oil through pipeline gathering, chemical engineering, nuclear energy plants, mixing and separating of gas-liquid, vehicle designers, environmental engineering, environmental pollution, metrologies, medical science, predict weather and warn of natural disasters, nervous system circulatory, the blood flow, civil engineering, simulation of all hydraulic engineering projects.

There are some advantages of CFD method when you compare with the experiment-based method of fluid system design, like, the rapidity of computing is very high compared with experimental studies, low cost; CFD analysis is cheaper than installing an experiment.

3.2.1 CFD Simulation Process

CFD codes are formed into structure with the numerical algorithm which deals with the problems of flow of the fluid. In order to issue easy access for the results, all commercial CFD packages include a streamlined and functional user interface to put in problem parameters and to check the results. The three ways to study fluid flow which are numerical, experimental and analytical.

These codes contain three major elements namely; pre-processor, solver, and post-processor, as shown in figure 3.1 which explain the following subsections.

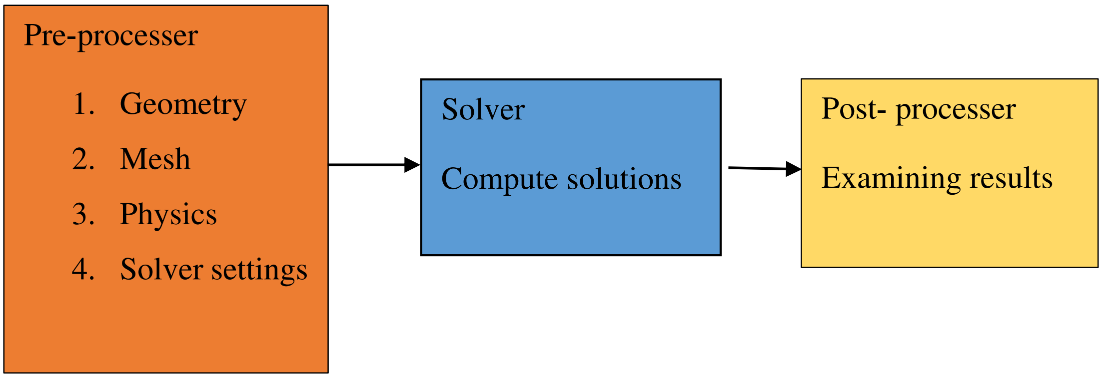

Figure 3.1 Progress of CFD Simulations

3.2.1.1 Pre-processor

The first step in formation and research of flow model is the pre-processor. It comprises of input of a flow problem via an operator, friendly interface which is followed by the modification of this input to a structure which is reasonable for the utilization by the solver. The user activities during pre-processing consist of the following stages: (i) describing the geometry of the computational domain, (ii) mesh (grid) has to be generated in order to divide the fluid domain in to smaller numbers, (iii) fluid properties acting on the domain, (iv) the specification of boundary conditions should be defined. Presentations are made at the nodes inside each cell with unknown flow properties like (velocity, pressure, temperature). The amount of cells in the grid is determined by the accuracy of a CFD solution. Thus, the higher the amount of cells the better the exactness of the solution. To enhance the exactness of the solution ıts required to have computer hardware and calculation time. Both calculation time and computer hardware are determined by the high quality of the grid. Attempts are underway to create CFD codes that have (self) adaptive meshing capability.

3.2.1.2 Solver

The numerical solver is the essential element of the CFD process and contains the main part of the CFD process. The three different procedures of numerical solution techniques are finite difference method, Finite element method and finite volume method. The most convenient method in CFD codes is finite volume method like ANSYS FLUENT. The fluid of the governing equations of the fluid flow problem has obtained by using CFD code after discretizing and iteration until it converges. other words, the solution algorithm requires the following steps (i) the variety of unknown flow parameters of any mode should be converted to an easy function, (ii) In order to be discrete the unknown functions of flow parameters need to be changed to the numerical manipulation (iii) iterative method should be solved by all the equations. Thus, in this section, it also contains the definition of fluid properties such as (velocity, density, viscosity, etc.) and the Selection of flow models.

3.2.1.3 Post-processor

This is used to describe how to carry out flow field visualization and get quantitative and /or qualitative data analysis on your CFD results in CFD-Posts. CFD-Post contains many tools such as streamlines, animation creation, XY plotting, rotating domain translation, vector plots, velocity profile, scaling, velocity, contour plots, pressure, kinetic energy, separating the region of the domain by color and other flow properties.

3.3 Turbulence

Turbulence is the time-change turbulent behavior which is found in a great deal of fluid flows. In general, its believed that as a result of the inertia of the fluid of a body: the peak of time vary and convective acceleration; thus flows that have small inertia effects are likely to be laminar (the Reynolds number estimates how much inert affected the flow). Speculations are, even though it's not clear, that turbulence is properly detail by the Navier-stokes equations.

The analytical results for the stormy flow of the N-s is pretty challenging, also as a result of such remarkably contrasting mixing-length scales that play an important role in stormy flow, the rational results of this demands such a fine mesh resolution that the time of computation turns to highly practical for calculation. Efforts to compute turbulent flow by the use of laminar solver usually lead to a time-unsteady solution, which falls short of connecting properly. To combat this, time-averaged equations like the RANS equations, boosted with turbulence models (such as the k-ε model), which can be used in experimental CFD applications in modeling the flows of turbulent. A different way for solving arithmetically of the N-s equations is the LES. This viewpoint is arithmetically costlier than the RANS method (both in computer memory and time), but initiates satisfactory outcomes as long as the larger turbulent scales are definitively determined.

3.4 CFD Turbulence Models

For all kinds of fluid flow can be applied by CFD modelling. In comparison with turbulent flow the investigation of a laminar flow is much easier, which requires a few especial analyses for modeling. The ANSYS FLUENT software gives various alternatives of multiphase models like volume of fluid (VOF), Eulerain models and mixtures, which includes some models of turbulence such as, spalart-All Maras model, k-ω models, while k and ω stands for turbulence kinetic energy and specific dissipation rate, respectively. Another model of turbulence is k-ε models, where k stands for turbulence kinetic energy and ε is turbulence dissipation rate. The Reynolds stress models, The V2-F model, (LES) Large Eddy simulation model and (DES) Detached Eddy simulation model. The chosen of any one of the above mentioned turbulence model depend on the type of flow pattern and fluid problems.

3.4.1 k – ω Turbulence Model

In this section two contrasting types have detailed, shear stress transport k – ω (SSTKW) and standard k – ω (SKW) utilize the same transport equations for k and ω. Nevertheless, SST varies in SKW model to some extent. The two of them are extensively used in the world. The k - ω model have received acclaim and its mainly because:

- The model equations don't include conditions that aren't defined at the wall, they can be jointed to the wall without utilizing wall function.
- They are precise and vigorous for a broad scope of boundary layer flows which have pressure gradient.

3.4.1.1 SST k – ω model

F.R. Menter in (1994) created the shear stress transport (SST) k – ω model by utilizing the standard k – ω model and transformed k -ε model. The SST k – ω model use a function that fuses together to steadily transform from the (SKW) model close to the wall and also a large Reynolds number model of the (k-ε) model in the exterior part of the border layer. It requires adjustable turbulent viscosity model to describe the transport effect of the basic turbulent shear stress.

3.4.1.2 Standard k – ω model

Wilcox (1998) created standard k – ω model which was produced to improve the computation for Lower Reynolds number results, shear flow spreading, and compressibility. The two terms of transport equations k and ω standing for turbulent kinetic energy and specific dissipation rate in that order. It's used broadly in the fields of turbo-machinery communities and aerospace. Various sub-models of k – ω are shear flow corrections, compressibility effects and transitional flows. This model has been changed in an effort to enhance its accuracy.

3.5 Simulation and Modeling Procedure

Numerical simulations of flow around cylinders have been investigated by several programs, many of these computer programs are commercially available and very popular. In this simulation ANSYS FLUENT version 19. On core i7 computer Asus was utilized to perform the analyses. ANSYS is general aim software, that can be used to simulate interaction of all practice of physics, structural mechanics, fluid dynamics, electromagnetic, vibration and heat transfer. All kinds of turbulence models are used like SST k – ω model, standard k – ω, standard, Realizable k-ε, standard k-ε, Reynolds stress model, LES, DES, spalart-All Maras model.

Fluent is applied for the design and research aims in areas of fluid like mechanical, civil engineering, chemical and environmental engineering. İn order to compute the needed results it must be defined the geometry, mesh and solver setting. There are six important stages in ANSYS FLUENT software which are create geometry, check geometry, extract flow volume, mesh geometry, perform CFD and investigate the result.

3.5.1 Geometry and Boundary Condition

Flow field and boundary conditions for the likeness of the flow around circular, square and elliptical cylinders are shown in figure 3.2. The square and circular cylinder have been simulated with the characteristic length scale of 1m (D), while the elliptic cylinder is used with axis ratio of 0.5, in direction of fluid flow. The center of the cylinders is set at L_1= 15D from the upstream edge, L_2= 50D from the downstream edge and W/2= 4D from each side of the flow domain. Longitudinal uniform velocities ranging from $2*10^{-6}$ to 10 are put at the inlet of the flume, which is equivalent to the Reynolds number varying from 2 to $10*10^{6}$. Pressure outlet with an average (gauge) pressure of zero Pascale is set by the outlet boundary of the channel. The two sides of the channel and the cylinder walls have no-slip boundary condition, whereby the wall surfaces have velocity of zero and increases the velocity as it moves away from the boundaries.

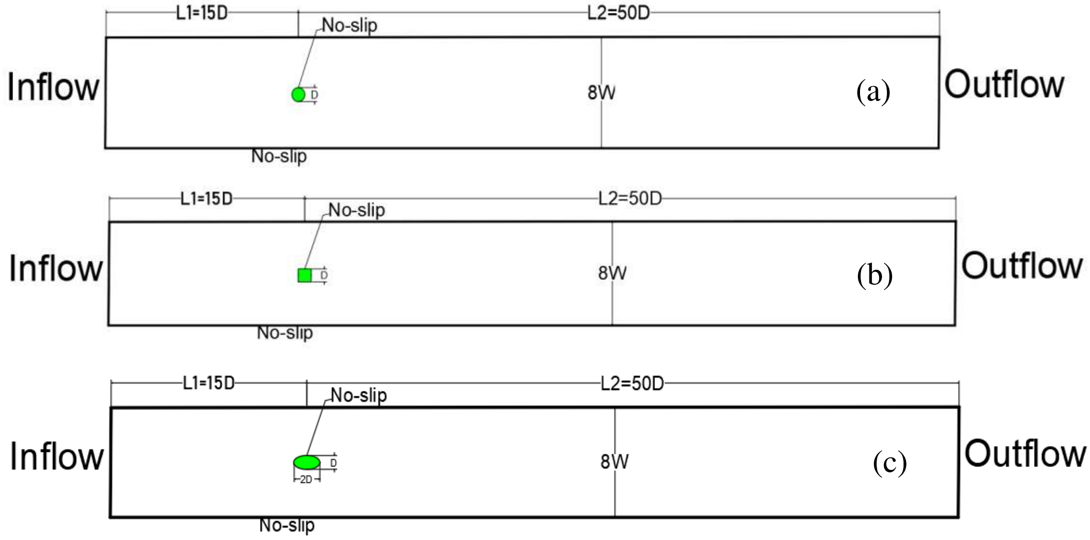

Figure 3.2 Simulation of (a) circular, (b) square and (c) elliptic models, and their boundary conditions

3.5.2 Meshing

Mesh independency study should be selected in order to get optimum mesh size. In this analysis the mesh is consisted of curvature and proximity. The size of the grid cells has directly impact to the outcome of the result. Therefore, the more grid cells you have the better results you receive. The mesh cells utilized in this analysis were refined to solve boundary layer separation and the wake behind the cylinders in to form of vortex street. Mesh is very important to get perfect boundary layer solution, sufficient number of nodes and very fine mesh can be done within the boundary layers. The mesh of the computational domain for circular, square and elliptical cylinders are shown in figure 3.3. The quality of mesh is also shown in figure 3.4. In the mesh quality the worst cells have an orthogonal quality nearer to 0, while the best cells nearer to 1. in order to enhance the exactness of the analysıs results 207797 elements and 209277 nodes were used in the computational domain.

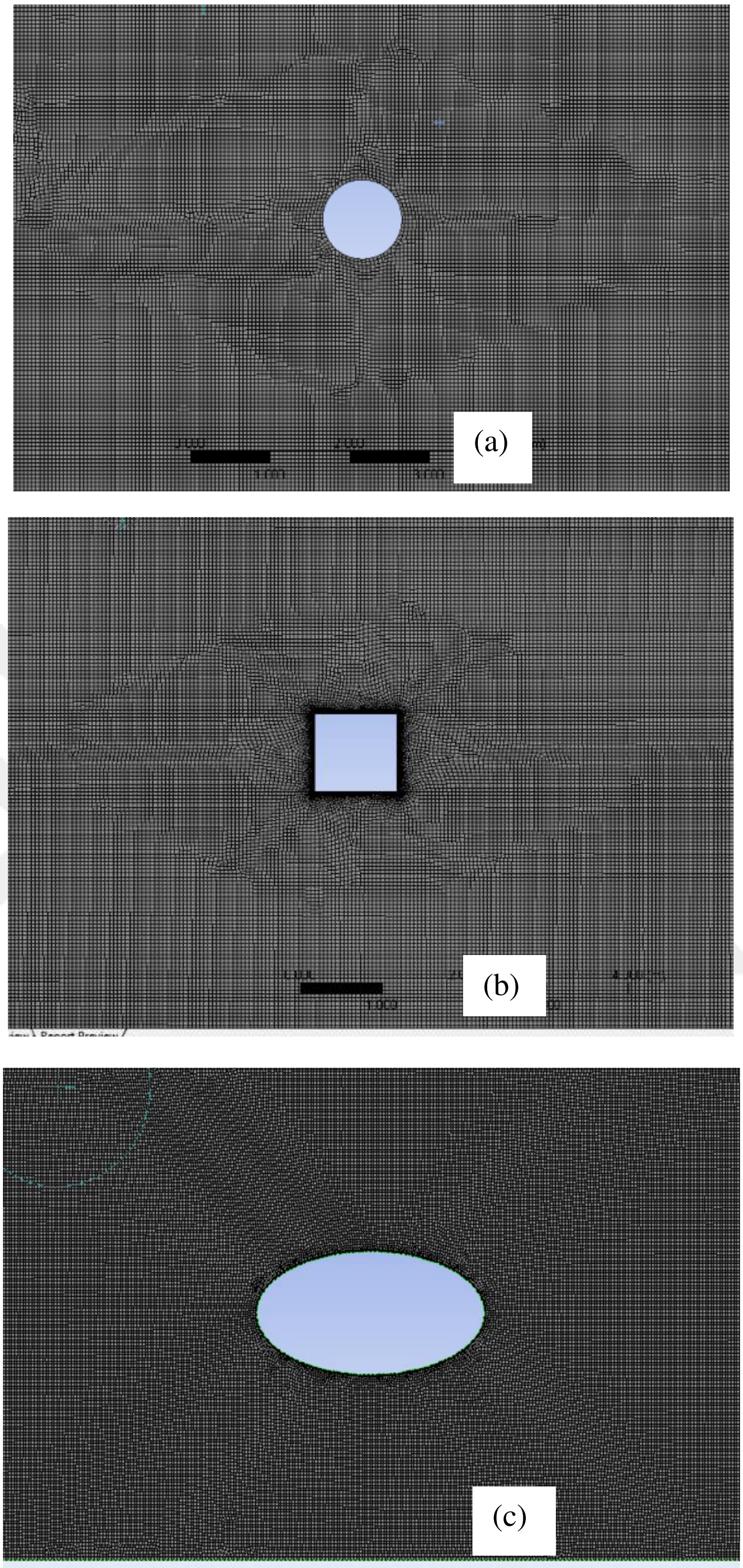

Figure 3.3 Meshing computational domain of (a) circular, (b) square and (c) elliptic cylinders

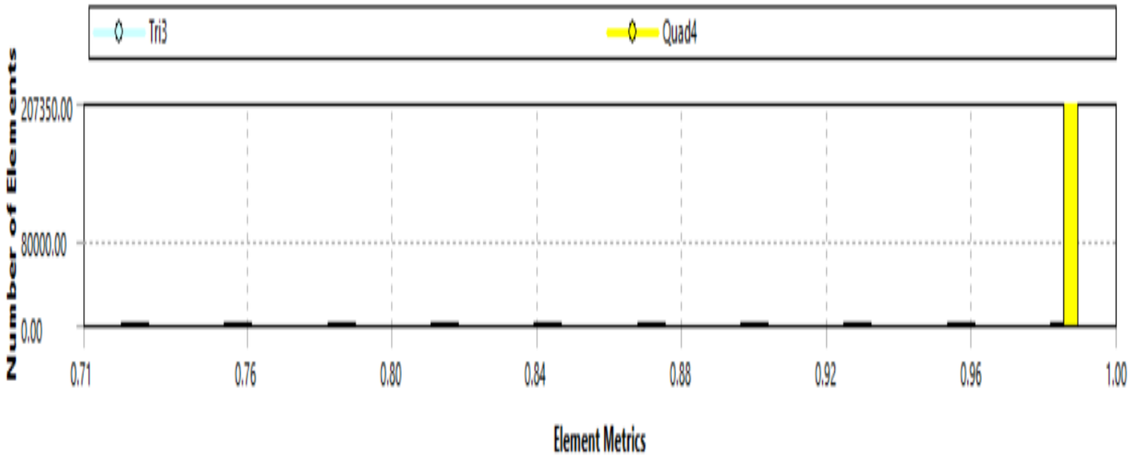

Figure 3.4 Quality mesh of the analysis

3.5.3 Solving the model and initialization

In this section, the turbulence properties are inserted and determined. The inlet is accepted as starting point to initialize the solution. The inlet velocity in the x-direction ranges from $2*10^{-6}$ m/s to 10 m/s corresponding Reynolds number ranges from 2 to 10^7. The number of iterations is set to be 3000 for good convergence. Figure 3.5 shows Reynolds number versus residuals.

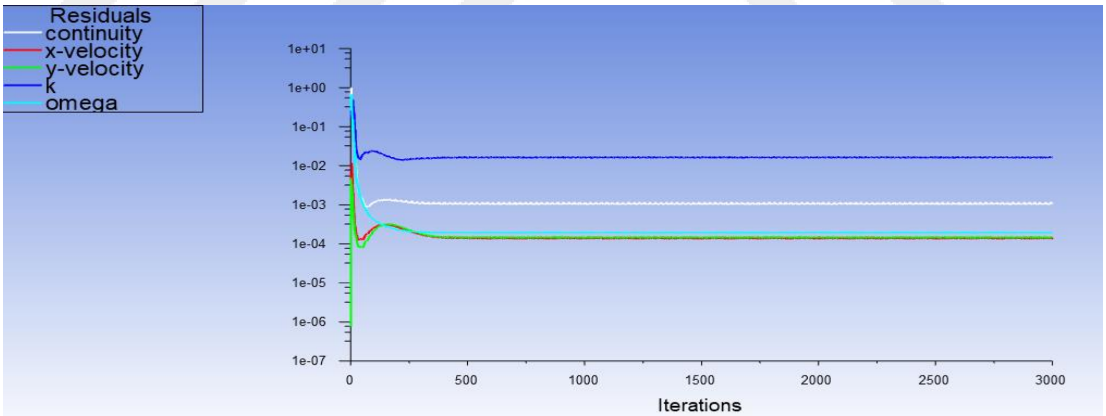

Figure 3.5 Number of iterations versus the residuals

CHAPTER 4

RESULTS

4.1. Introduction

The numerical simulations of flow around circular, square and elliptic cylinders have been implemented for wide range of Reynolds numbers of 2, 4, 15, 38, 160, 190, 250, 290, 10^3, 10^4, 10^5, $2.5*10^5$, 10^6, $1.5*10^6$, $2*10^6$, $3*10^6$, $4*10^6$, $5*10^6$, $8*10^6$, $9*10^6$ and 10^7, as shown in Table 4.1. Water temperature was set to be 20^0C, Reynolds number was calculated by Equation 4.1.

$$Re = \frac{\rho V D}{\mu} \tag{4.1}$$

Table 4.1. The flow conditions of the simulations

Cases	Reynolds number	Velocity flow (m/s)
1	2	$2*10^{-6}$
2	4	$4*10^{-6}$
3	15	$1.5*10^{-5}$
4	38	$3.8*10^{-5}$
5	160	$1.6*10^{-4}$
6	190	$1.9*10^{-4}$
7	250	$2.5*10^{-3}$
8	290	$2.9*10^{-3}$
9	10^3	10^{-3}
10	10^4	10^{-2}
11	10^5	10^{-1}
12	$2.5*10^5$	0.25
13	10^6	1
14	$1.5*10^6$	1.5
15	$2*10^6$	2
16	$3*10^6$	3
17	$4*10^6$	4
18	$5*10^6$	5
19	$8*10^6$	8
20	$9*10^6$	9
21	10^7	10

4.2 Simulation of Flow Around Circular Cylinder

4.2.1 Velocity Streamlines

A family of curves which are tangent to the velocity of vector flow at any instant in time is called streamlines. The streamlines show the immediate direction in which a fluid element is going to travel. In steady flow the path lines, streamlines and streak lines coincide. For the Reynolds number (Re) 2 and 4 the flow will not produce turbulence and the streamlines remain straight and parallel to one another. When the Re increases in the flow approaching the cylinder, the transition of flow from laminar to turbulence takes place and the flow turns into unsteady because of the resistance forces. The wake flow observed in the downstream region due the flow of fluid around cylinders contains vortices. Figure 4.1 shows the velocity streamlines for several Re.

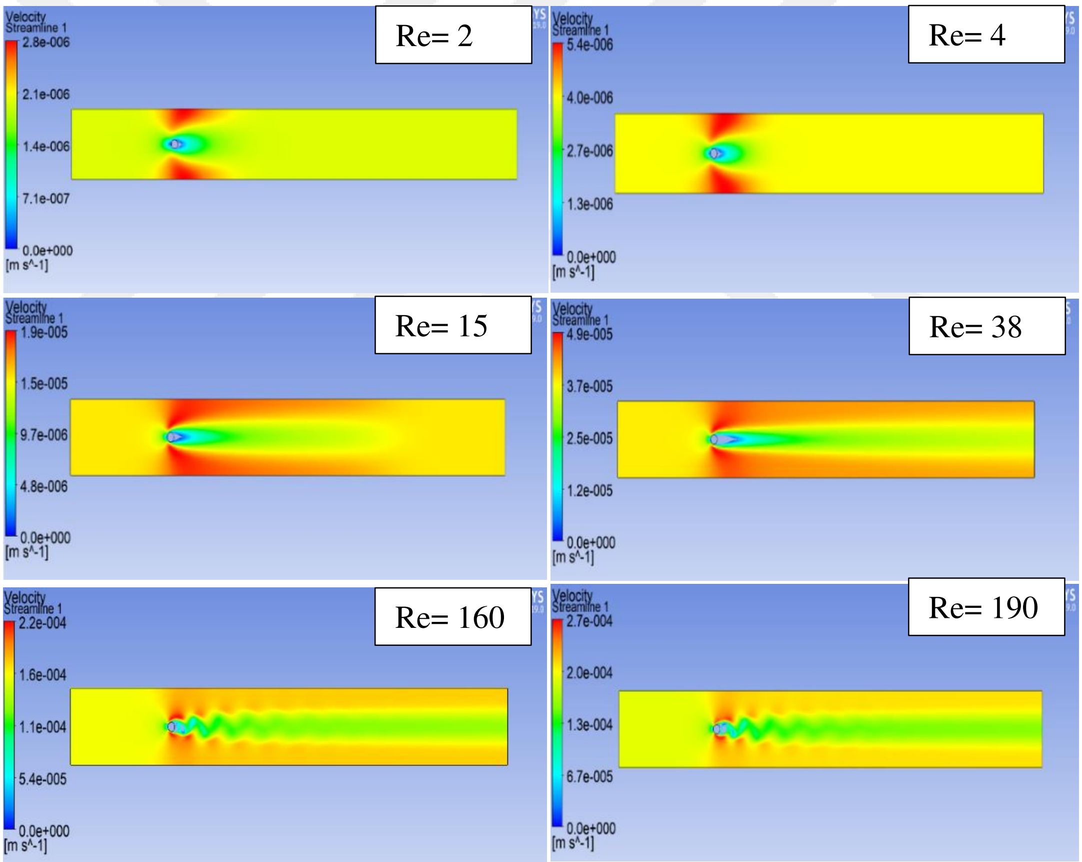

Figure 4.1 Velocity streamlines

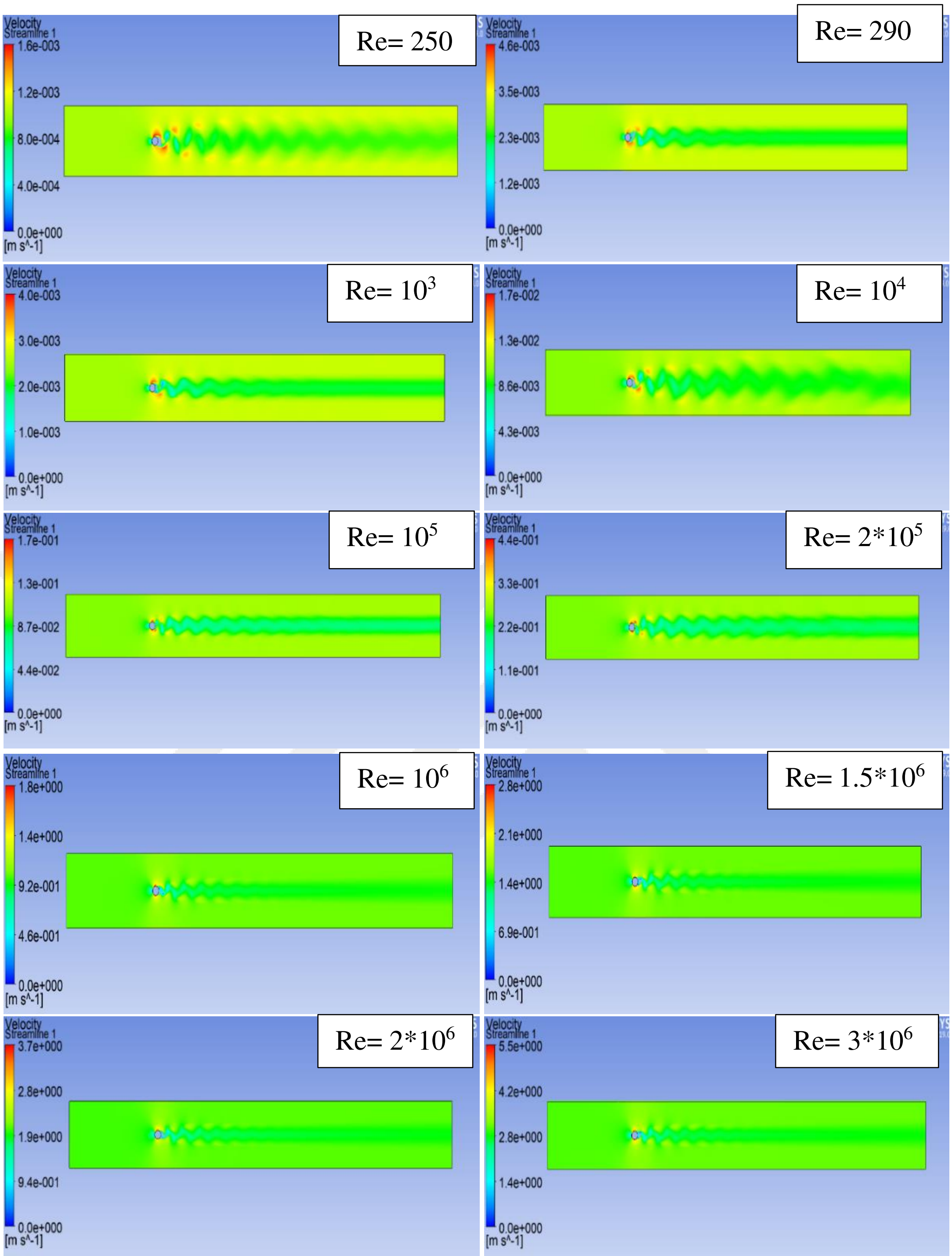

Figure 4.1 (Cont.) Velocity streamlines

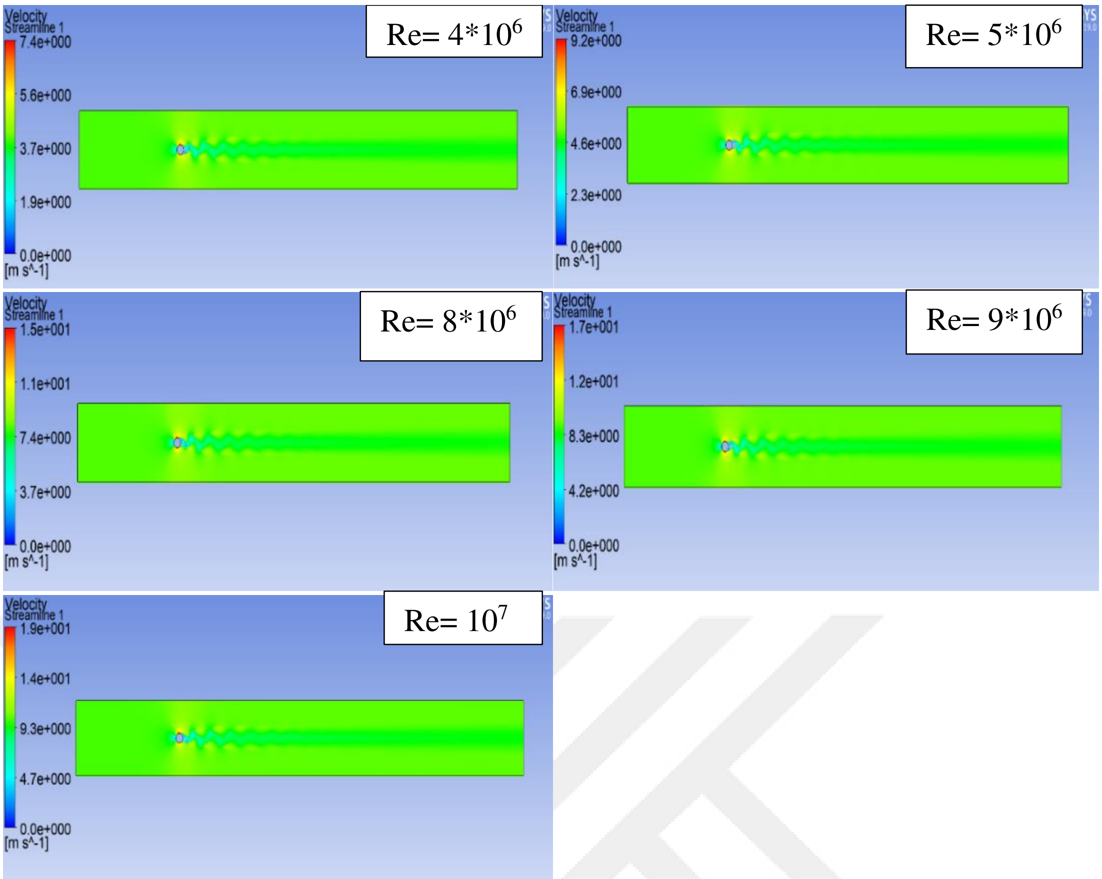

Figure 4.1 (Cont.) Velocity Streamline

4.2.2 Flow Regime

In this part, we will talk about the flow regime around circular cylinder for various Reynolds number. In table 4.1 gives the information on all cases in order to observe different flow field. Figure 4.2 illustrate the velocity streamlines and velocity contour from the simulation. CASE1 and CASE2 (creeping flow without separation) agree to flows with low Reynolds number ($Re < 5$), also their streamlines perfectly symmetrical from the upstream to downstream of the circular cylinder. CASE3 and CASE4 (a constant couple of symmetric vortices) $5 < Re < 40$, in figure 4.2 illustrate the near wake of the velocity (streamline and contour), for the ($Re = 15$ and 38) a fixed pair of upper and lower vortices was produced in the wake behind the cylinder. When Re increases the length of the vortex region is widened. In CASE5 and CASE6 ($Re = 160$ and 190) von Karman vortex street takes place. In this case the vortex firstly developed in one side of the cylinder and increased again in another side of the cylinder. CASE7 and CASE8 ($200 < Re < 300$) transition to turbulence in the wake is occurred. This transition range of regime is known as irregular range. The turbulence is started by laminar to turbulent transition in the free layers which originated from the separation point on the cylinder. In figure 4.2 shows that, from CASE9 to CASE12 $300 < Re < 3*10^5$ (Wake become fully turbulent). The range of this Reynolds number ($300 < Re < 3*10^5$) is characterized as subcritical region. In CASE13 and CASE14 ($3.5*10^5 < Re < 1.5*10^6$) this scope of Reynolds number is described as supercritical region. As shown in figure 4.8 ($Re = 1*10^6$ and $1.5*10^6$) the separation of boundary layer is turbulent on the two sides of the circular cylinder. In CASE15 and CASE16 $1.5*10^6 < Re < 4*10^6$, fully turbulent occurs at one side of the boundary layer. This regime is known as upper-transition flow regime. Finally, when Re increased $4*10^6 < Re$ it is called trans-critical, the two sides of the boundary layer become completely turbulent.

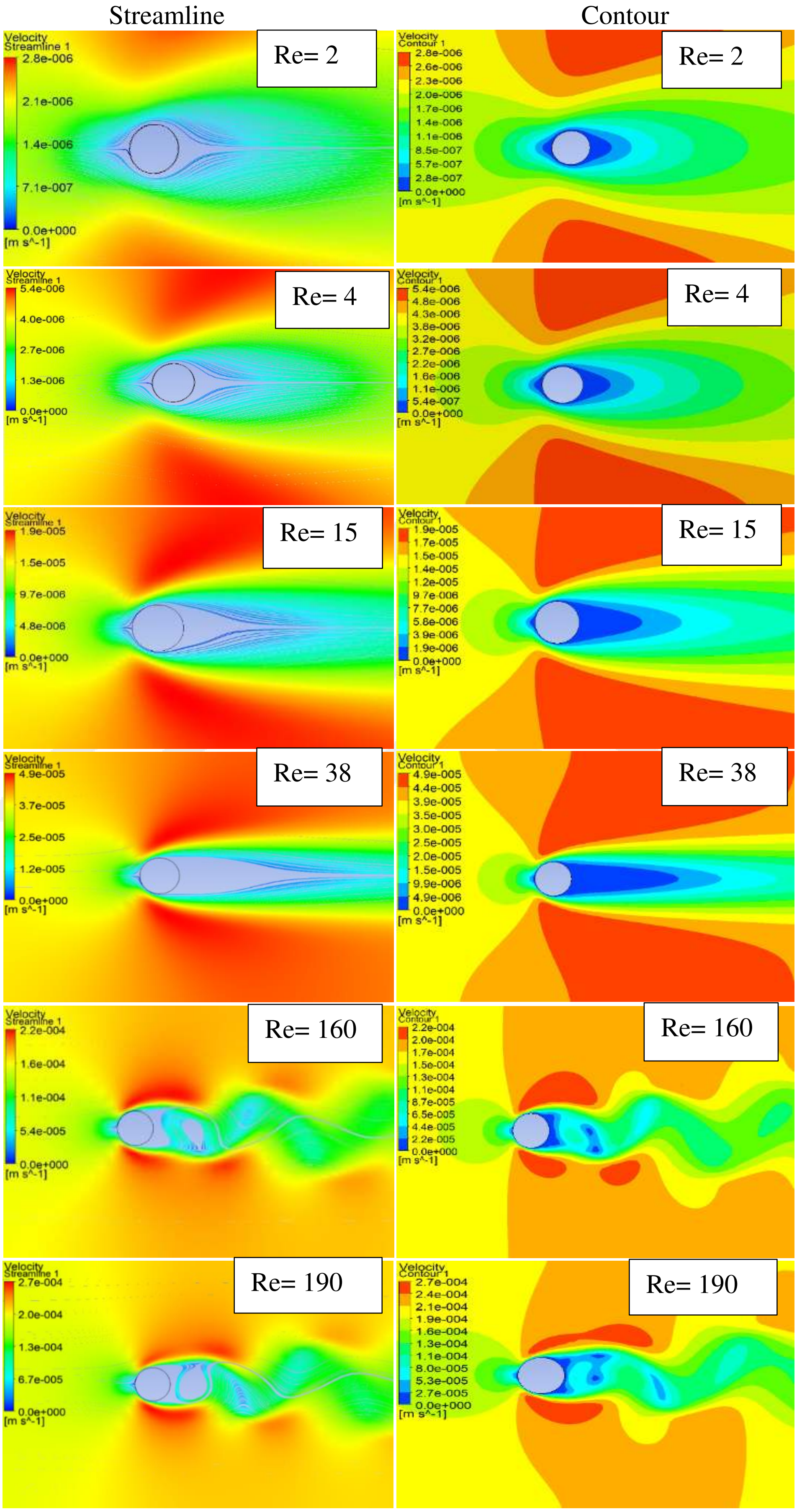

Figure 4.2 Flow around circular cylinder

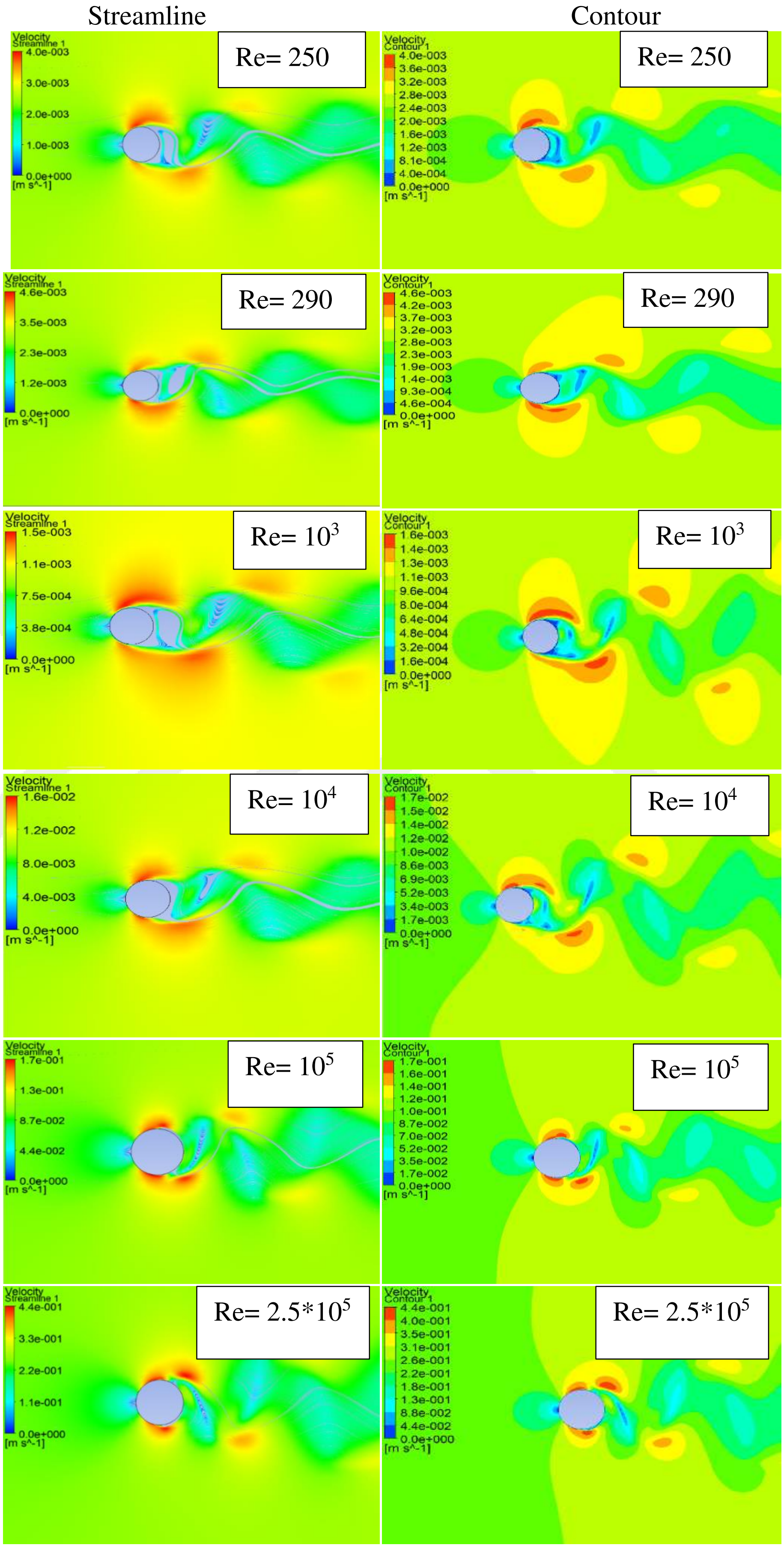

Figure 4.2 (cont.) Flow around circular cylinder

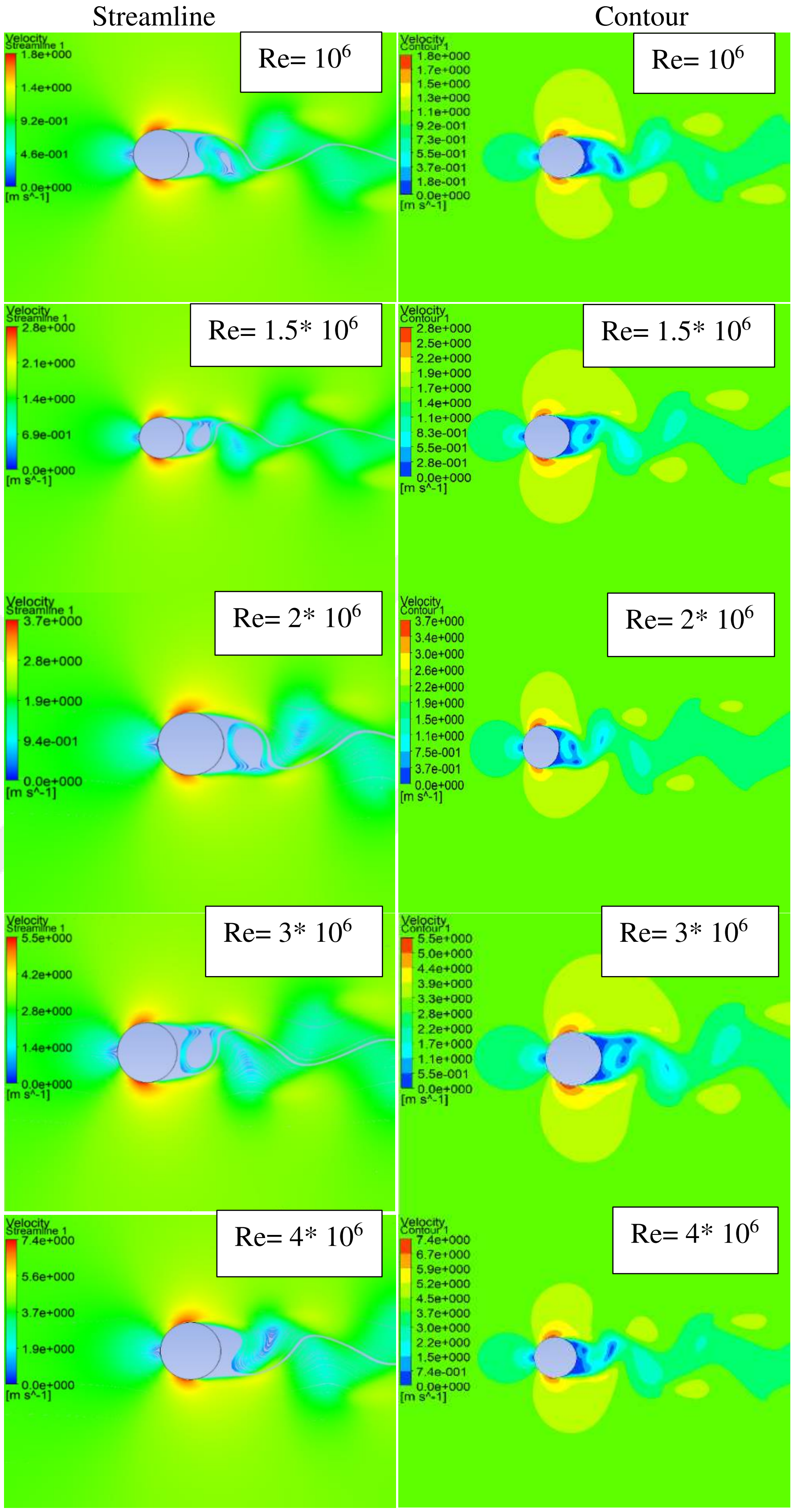

Figure 4.2 (cont.) Flow around circular cylinder

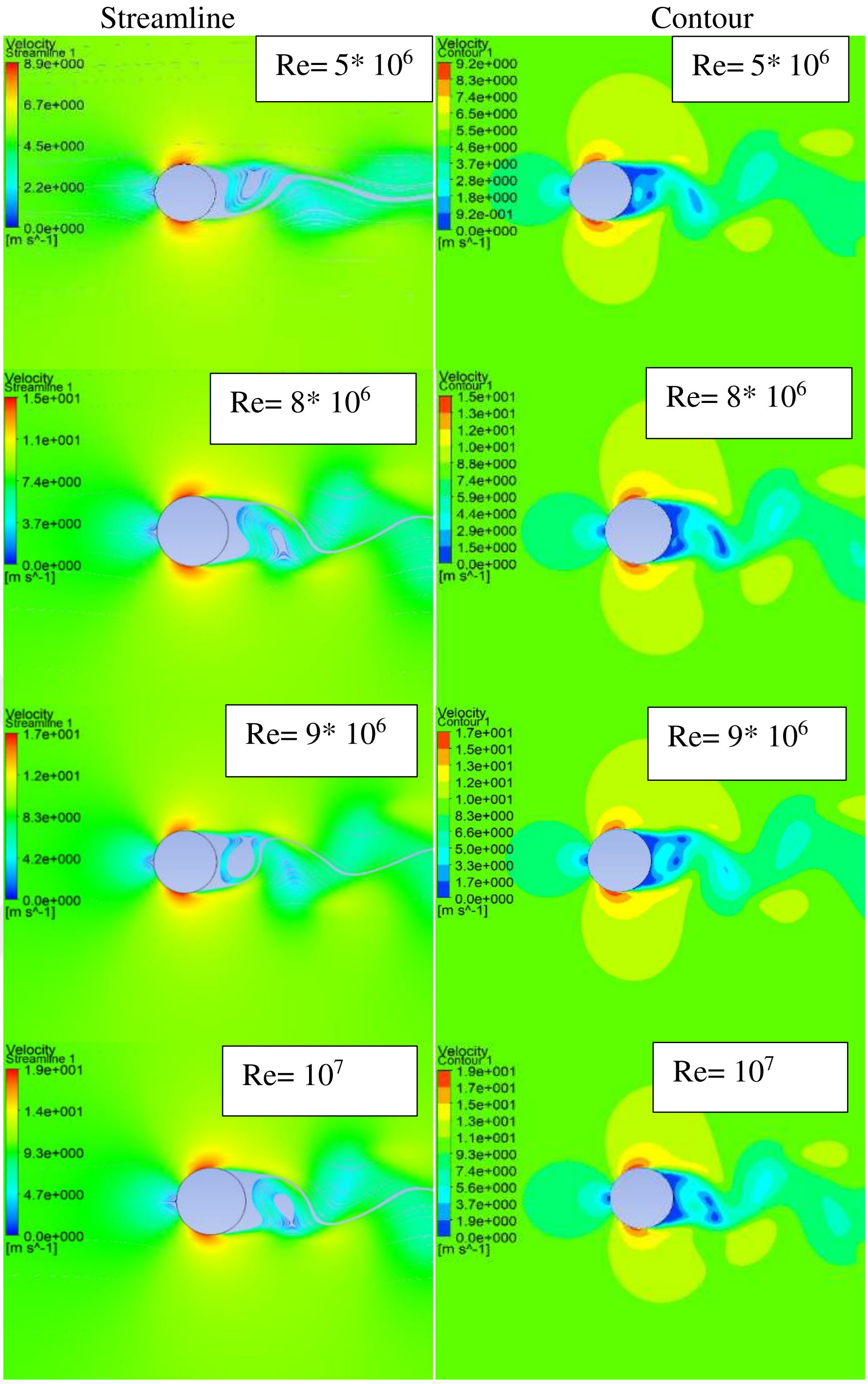

Figure 4.2 (cont.) Flow around circular cylinder

4.2.3 Velocity Profile

Length-wise velocity profiles (time-lines) of a flowing fluid in and around circular cylinders for an interval of Reynolds number are shown in figure 4.3. These time-lines indicate the velocity of the flow along a straight line in the horizontal direction which flows through the water surface of an open-channel. The velocity profiles appear to show stream flow of contrasting longitudinal distances from the cylinders. These distances are 15m, 12m, 9m, 6m, 4m, 3m, 2m and 0.5m of the upstream and 0.5m, 1.5m, 2.5m, 3.5m, 5m, 6m, 7m, 10m, 15m, 20m, 25m, 30m, 35m, 40m and 48m of the downstream of the cylinder. As for the flow field near the cylinders, the stream flow velocities reduce because of the existence of the obstacles, both of the upstream and downstream. The effect of the Reynolds number on the flow around cylinders is clearly visible. As the Reynolds number rises the wake flow become unstable and its length at the downstream of the cylinders rises. Velocity profile obtained from the simulation is shown in figure 4.3. The categorization of the flow field around circular cylinders presented by Summer and Fredsoe (1997) is assessed in this study.

CASE1 and CASE2 in figure 4.3 shows that the flow around circular cylinder with Reynolds number of (2 and 4). The uniformity in the velocity profiles of the flow around circular cylinder was lost in the upstream and downstream of the obstacle. There is no separation of fluid flow took place in circular cylinder. In CASE3 and CASE4 the Reynolds number are (15 and 38). In the range of $5<Re<40$ a couple of right and left vortices was produced within the wake of the cylinder. In CASE5 and CASE6 the von Karman vortex street take place in the velocity profile as shown figure 4.3. The transition from laminar to turbulent occurred in CASE7 and CASE8. From CASE9 to CASE21 only turbulent can be seen in the wake behind the cylinder.

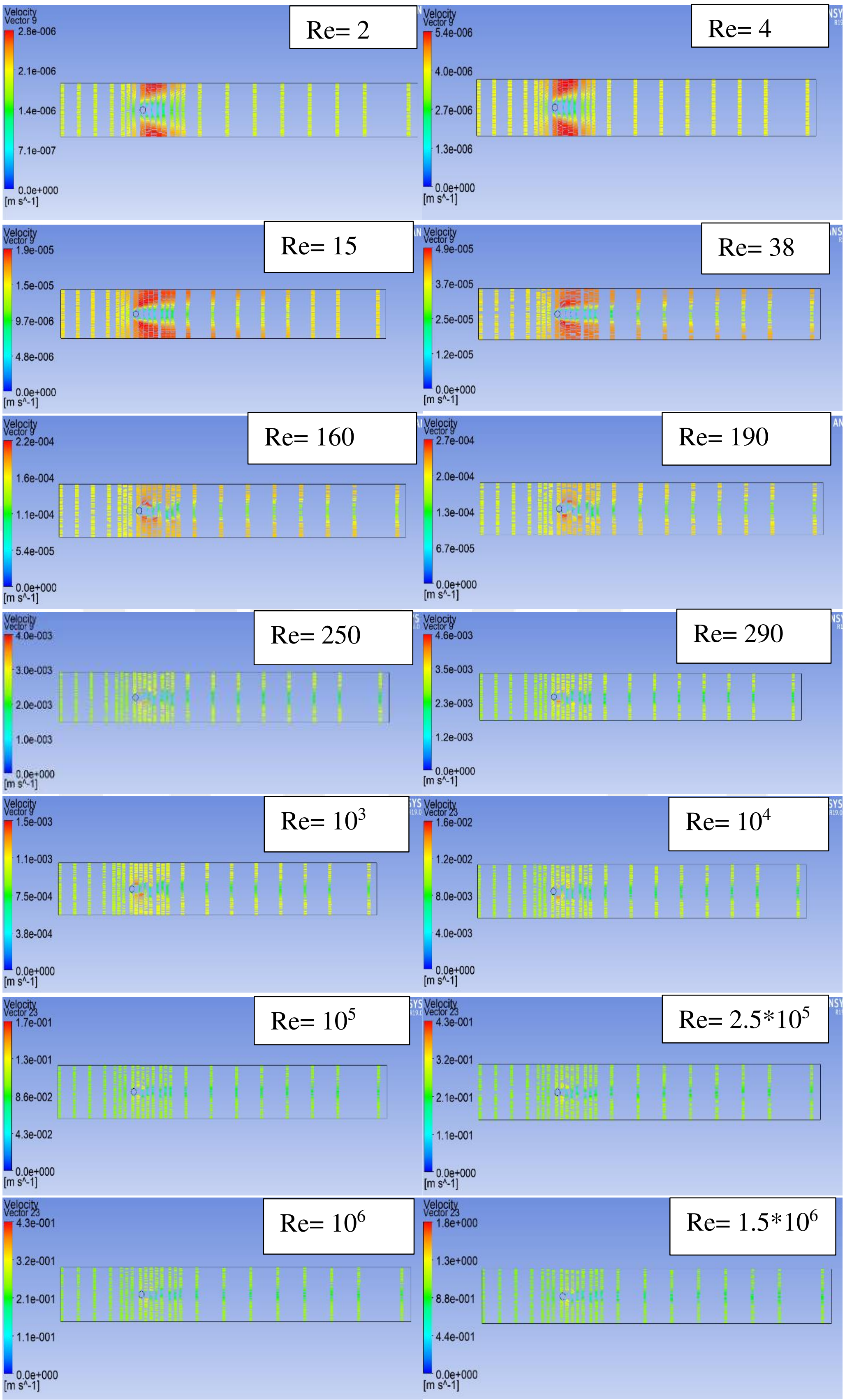

Figure 4.3 Velocity profile

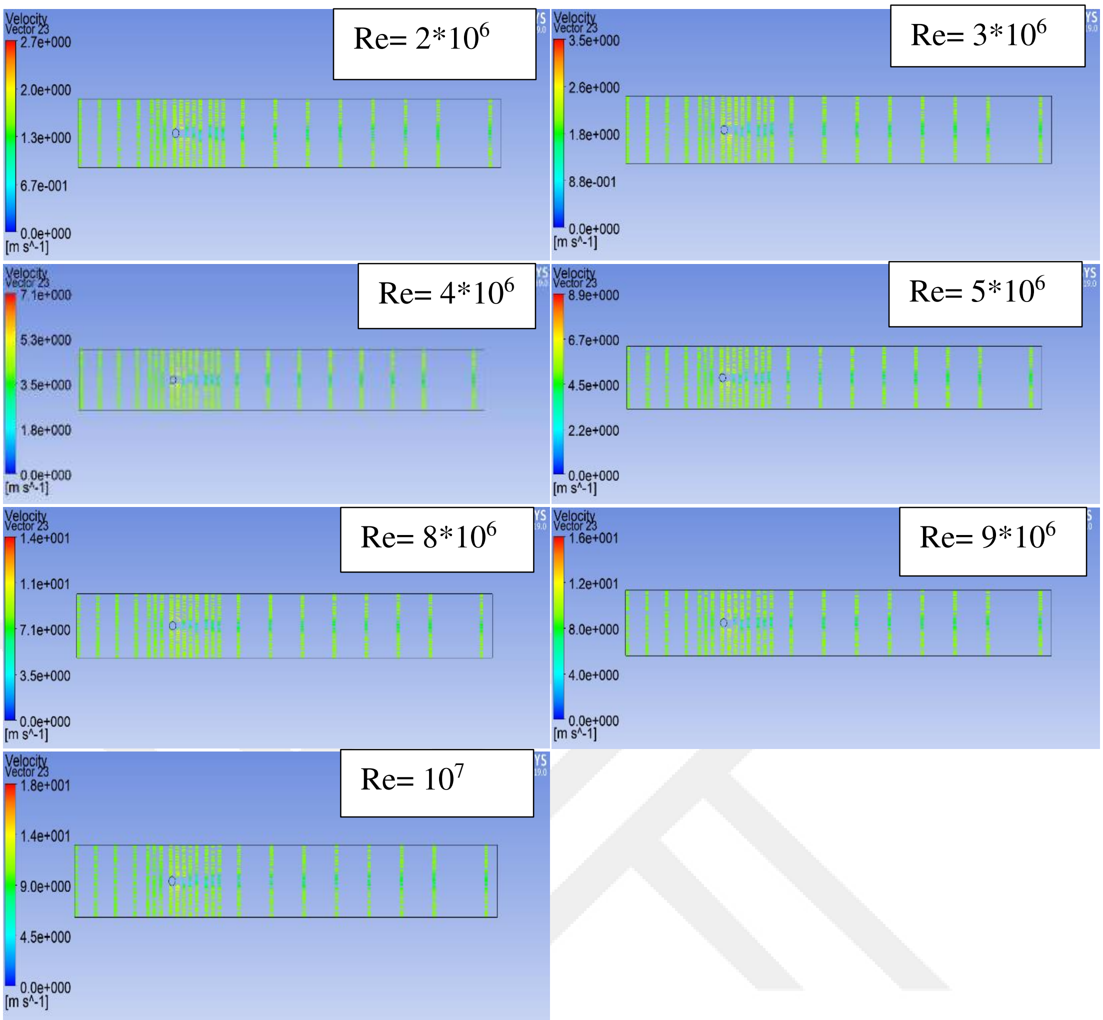

Figure 4.3 (Cont.) Velocity profile

4.3 Simulation of Flow around Square Cylinder

4.3.1 Velocity Streamlines

A family of curves which are tangent to the velocity of vector flow at any instant in time is called streamlines. These streamlines show immediately the direction in which a fluid element is going to travel. Figure 4.4 illustrates streamlines of the water flow around square cylinders for various ranges of Reynolds numbers. Moreover, the shape of the cylinders has significant influence on the flow field around the cylinders. It's important to know that the wake behind the square cylinder is much turbulent and enormous than the circular cylinder under the same flow conditions. İn CASE1 and CASE2 for Reynolds number of 2 and 4<5 for the square cylinder a different separation points and different flow patterns is clearly observed.

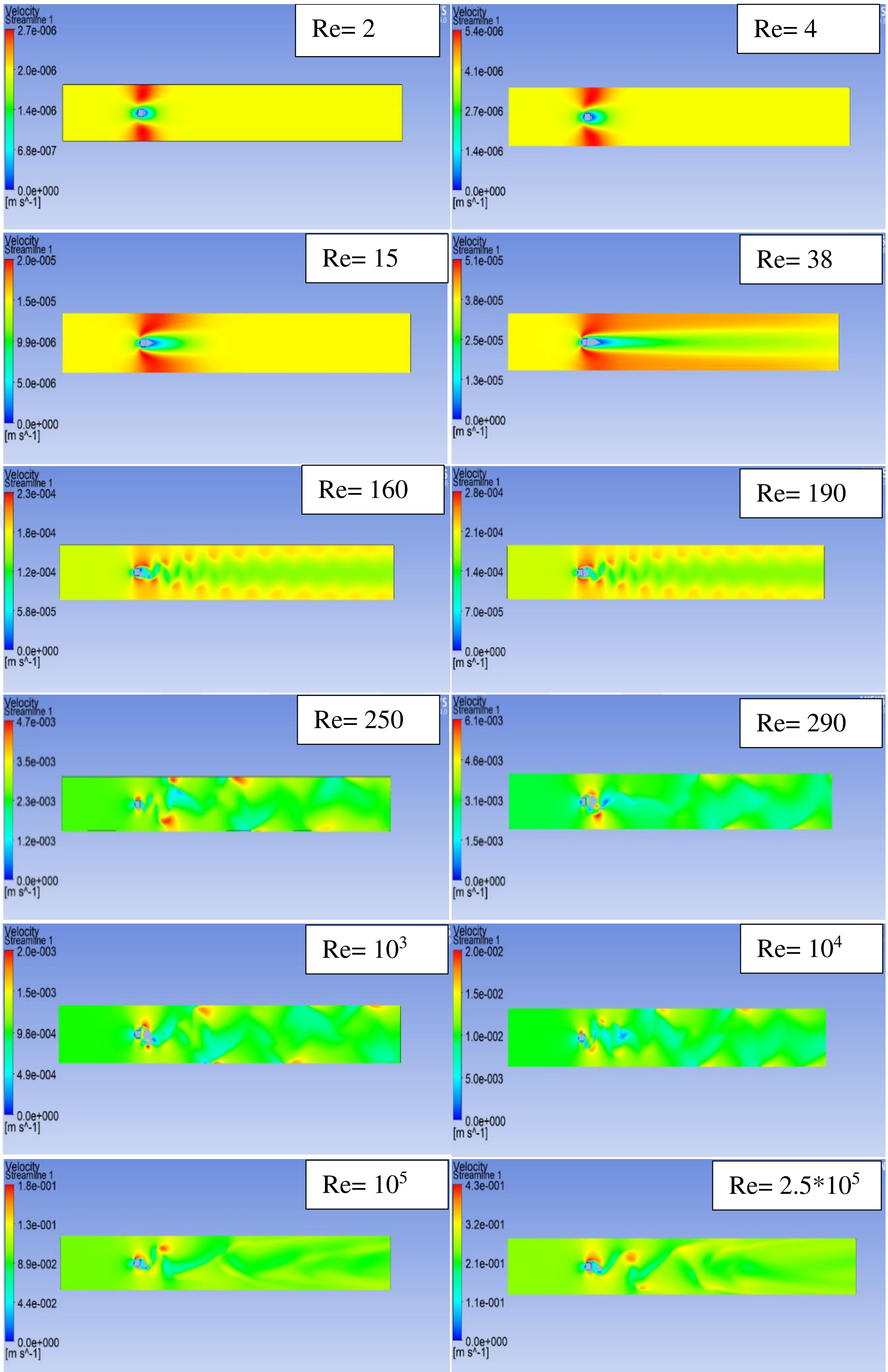

Figure 4.4 Velocity streamline

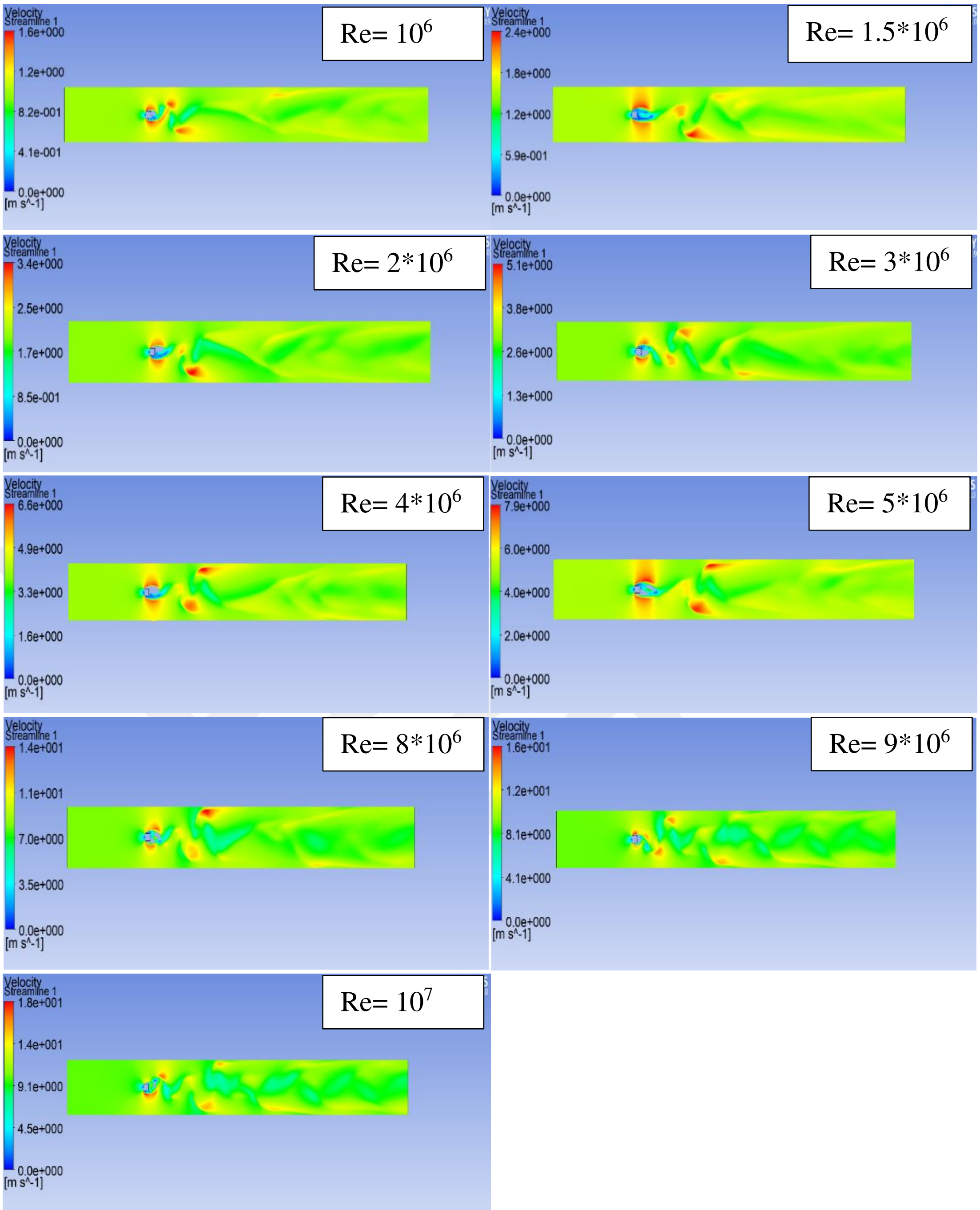

Figure 4.4 (Cont.) Velocity streamline

4.3.2 Flow Regime

In this part, we will talk about the flow regime around circular cylinder for various Reynolds number. In table 4.1 gives the information on all cases in order to observe different flow field. Figure 4.5 illustrate the velocity streamlines and velocity contour from the simulation. In CASE1 and CASE2 for Reynolds number of 2 and 4<5 for the square cylinder a different separation points and different flow patterns is clearly observed.

When the Reynolds number ıs expanded to 5 < Re (=15 and 38) < 40 a firm pair of symmetric vortices occur at the wake of the cylinders (CASE3 and CASE4). As shown in the figure, the vortex area of the cylinder is a little bit larger and longer compared to that of the circular cylinder. A pair of right and left vortices was produced inside the wake behind the cylinder, and the velocity is zero around a small area of the cylinder. When the Re is enlarged further to 40 < Re (=160 and 190) < 200 (CASE5 and CASE6), the von Karman vortex sheet occurs. As the Re increase 200 < Re (=250 and 290) < 300 (CASE7 and CASE8), the flow behind the square cylinder generates a broader wake than the circular cylinder. Broader wakes produce huge drag coefficient. As Reynolds number is enlarged further to 300 < Re (= 10^3, 10^4, 10^5 and $2,5*10^5$) < $3*10^5$ the wake flow behind the square cylinder becomes totally turbulent (CASE9 to CASE12). The wake flow behind the square cylinder proves to be exceedingly chaotic. Lastly, as Reynolds number is enlarged even further Re > $3*10^5$, the thickness of the wake flow behind the square cylinder becomes extremely thicker than the wake behind the circular cylinder (CASE13 to CASE21). Figure 4.5 shows the flow regime of square cylinder.

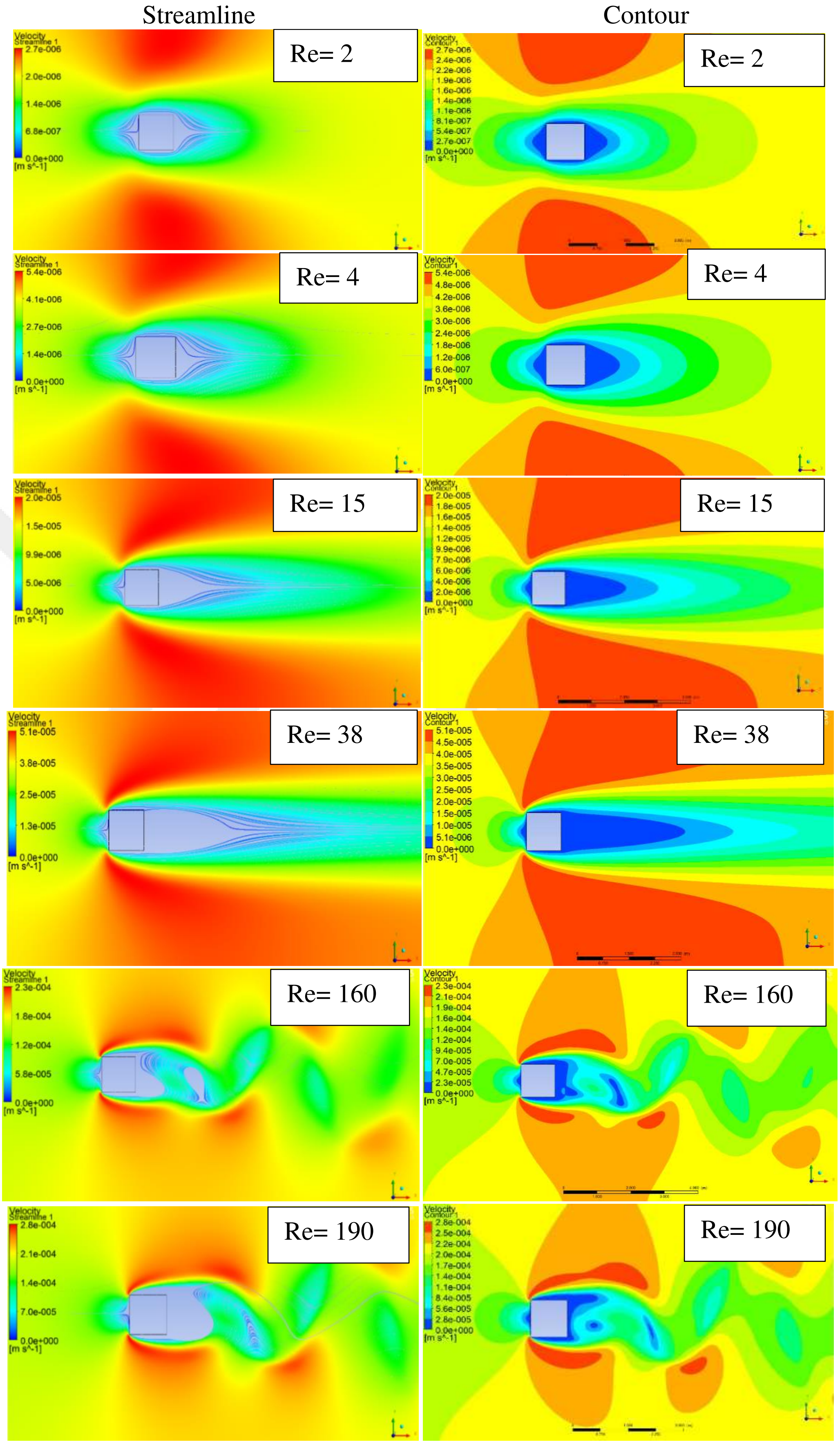

Figure 4.5 Flow around square cylinder

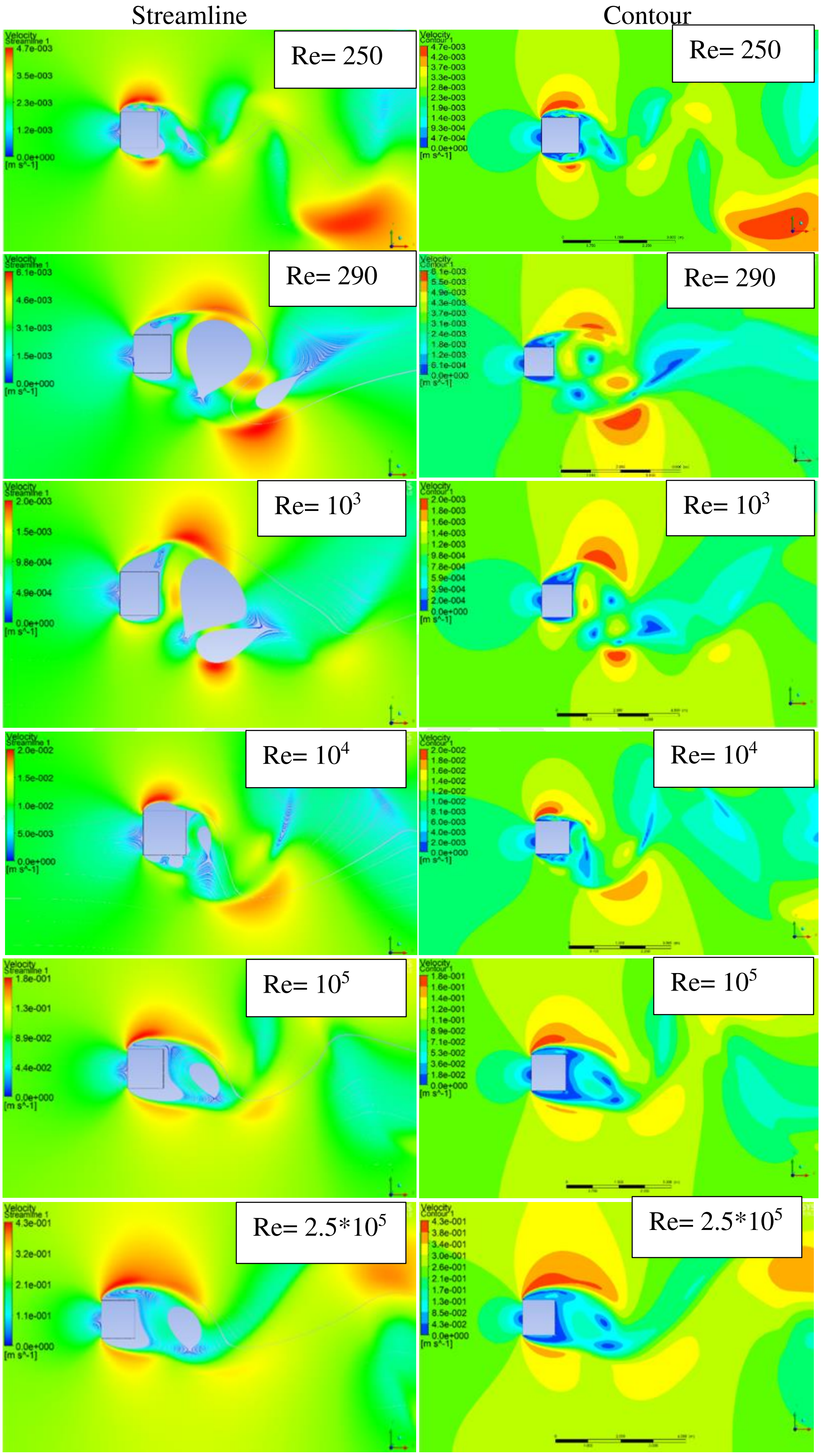

Figure 4.5 (cont.) Flow around square cylinder

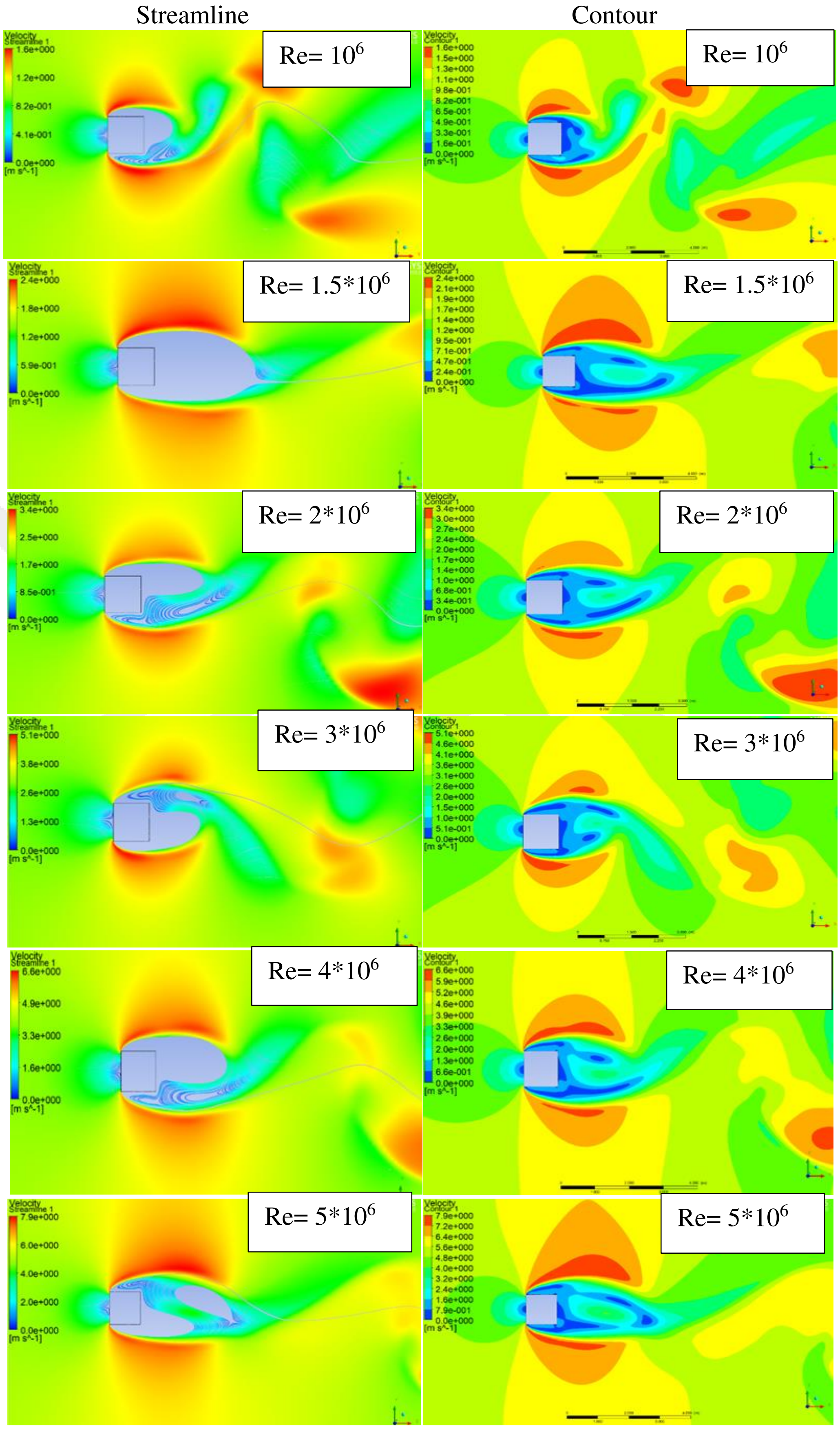

Figure 4.5 (cont.) Flow around square cylinder

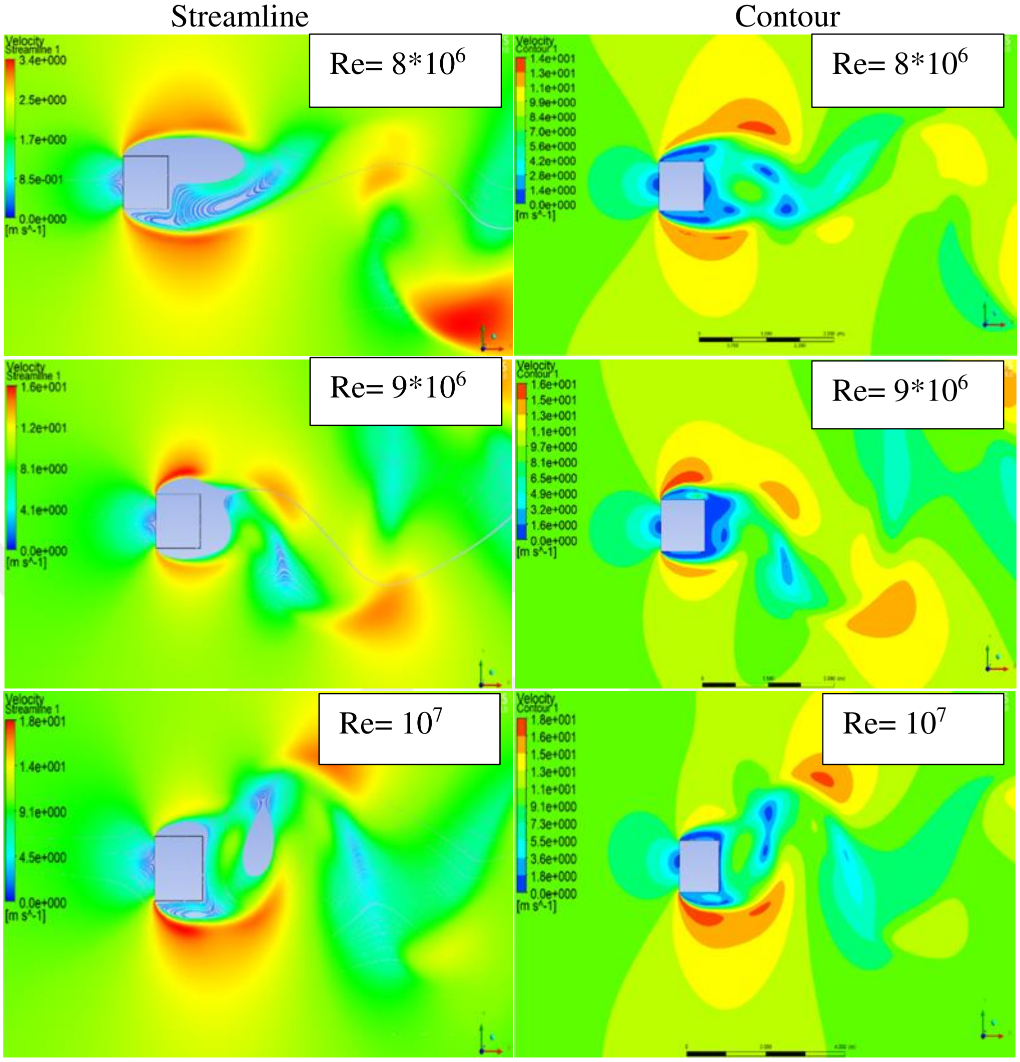

Figure 4.5 (cont.) Flow around square cylinder

4.4.2 Velocity Profile

The velocity profile for square cylinder are used the same interval as the circular cylinder which has already mentioned above. The rationale behind this is to compare the different compound phenomena with circular cylinder. The shape of square cylinder usually results a large and several regions of separated flow and huge unsteady wake region in the downstream. As the walls of the simulation domain applied no-slip conditions, the flow of the velocity is zero at boundaries. Velocity profile demonstrates that the walls has no influence or no impact on the flow around the cylinders. As its shown in figure 4.6 the velocity is slowly increases away from the walls.

CASE1 and CASE2 in figure 4.6 illustrates that the velocity profile of the fluid altered as the fluid approaches to somewhere around and about 3.5m downstream of the square cylinder. As Reynolds number increased $5 < Re < 40$ in CASE3 and CASE4, the velocity profile starts to establish the different magnitude velocity upstream, downstream and around the cylinder and produce a fixed pair of symmetry vortices behind the square cylinder. As Reynolds number increased further number $40 < Re < 200$ in CASE5 and CASE6, separation takes place the back corners of the cylinder and the flow becomes periodic. In CASE7 and CASE8 ($200<Re<300$), the flow start transition from laminar to turbulent. When Reynolds number increased for CASE9 to CASE21 the vortex shedding of square cylinder is longer and wider than the circular cylinder.

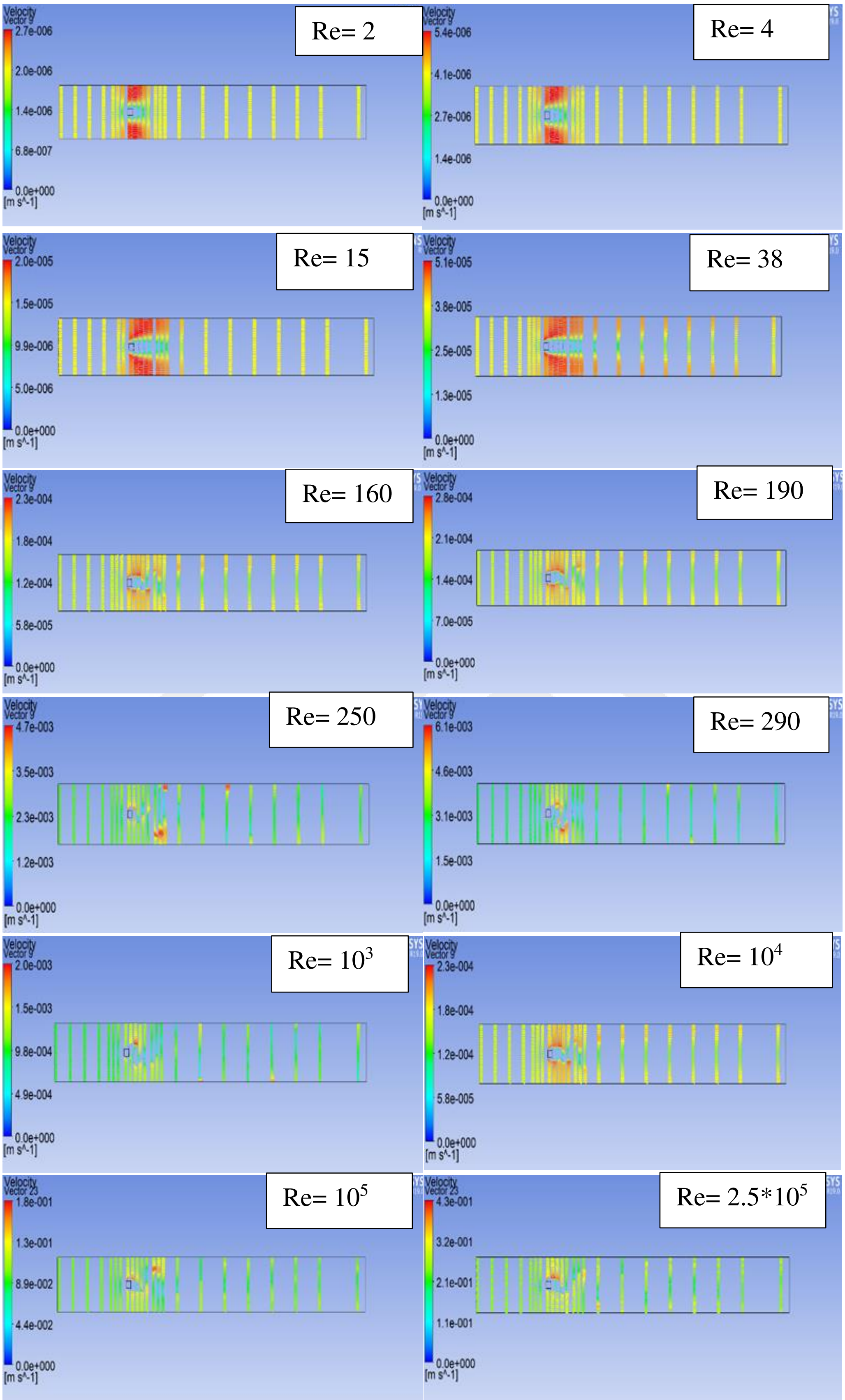

Figure 4.6 Velocity profile

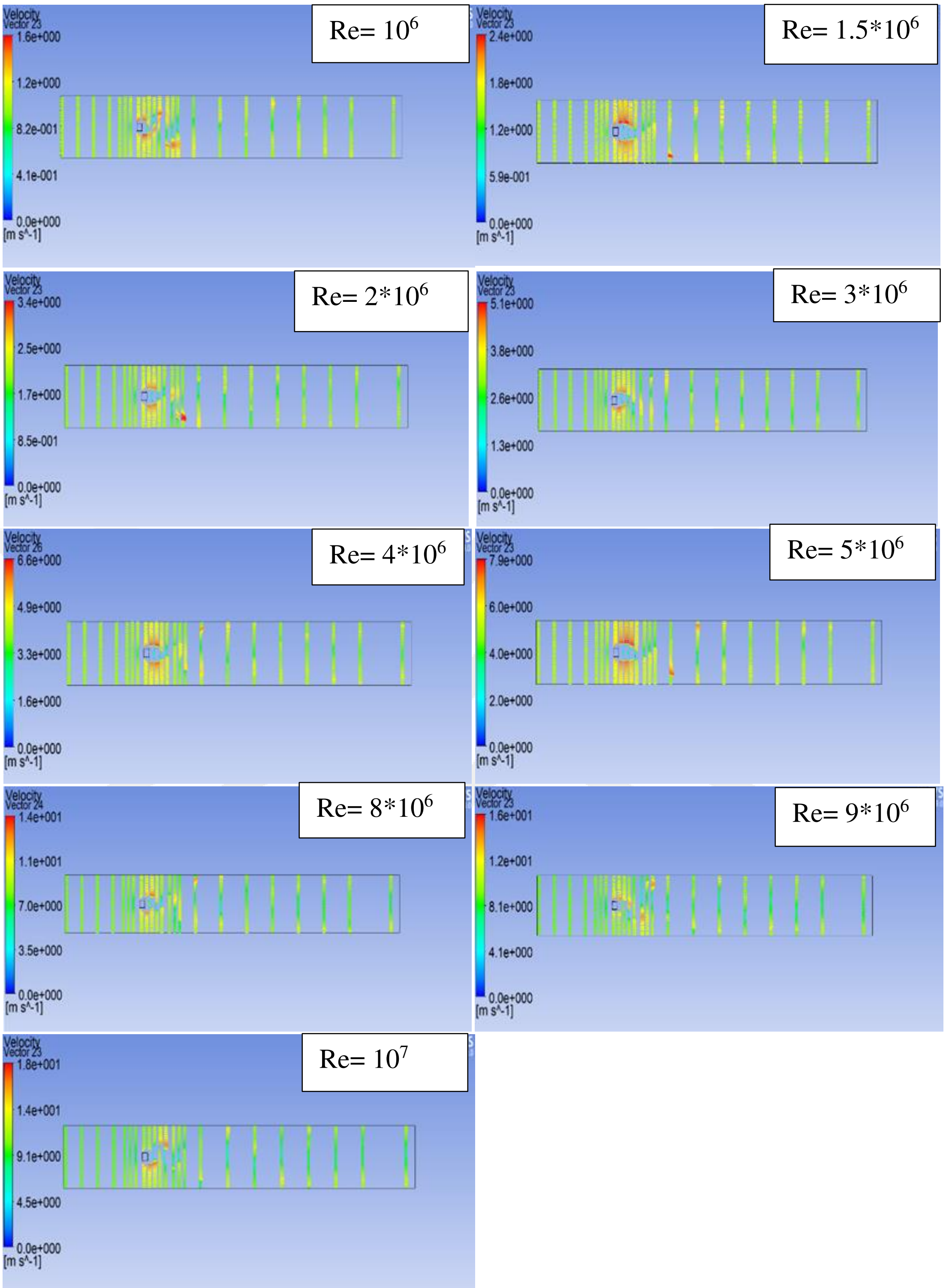

Figure 4.6 (Cont.) Velocity profile

4.4. Simulation of Flow Around Elliptic Cylinder

4.4.1 Velocity Streamlines

A family of curves which are tangent to the velocity of vector flow at any instant in time is called streamlines. These streamlines show immediately the direction in which a fluid element is going to travel. Figure 4.7 illustrates streamlines of the water flow around elliptical cylinders for various ranges of Reynolds numbers. Moreover, the shape of the cylinders has considerable effect on the flow field around the cylinders. It seems that the wake behind the elliptical cylinder is much turbulent than the circular cylinder until subcritical region under the same flow states.

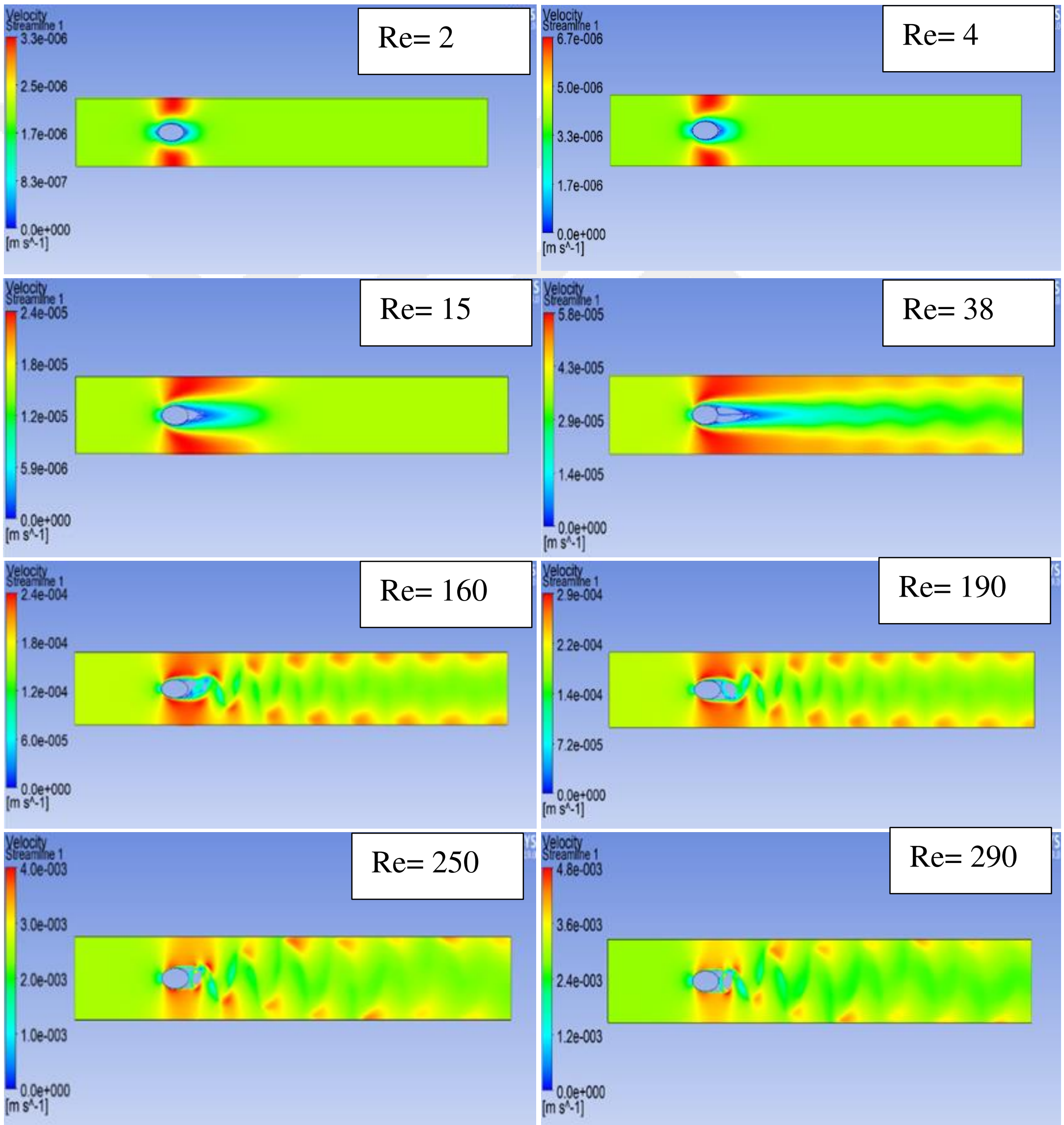

Figure 4.7 Velocity streamline

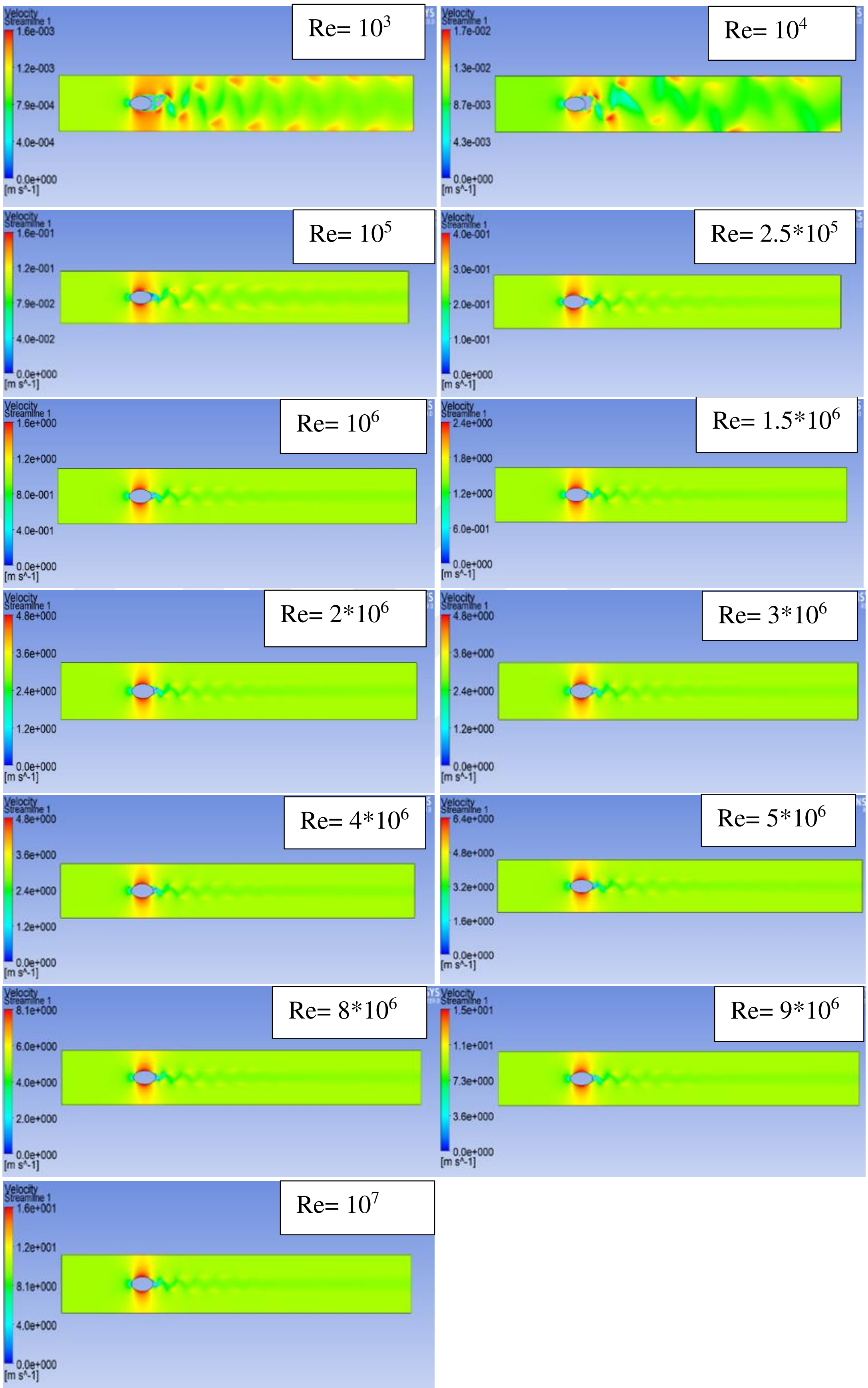

Figure 4.7 (con.) Velocity streamline

4.4.2 Flow Regime

In this section, we will talk about the flow regime around circular cylinder for various Reynolds number. In table 4.8 gives the information on all cases in order to observe different flow field. Figure 4.8 illustrate the velocity streamlines and velocity contour from the simulation. In CASE1 and CASE2 for Reynolds number of 2 and 4<5 for the elliptical cylinder a different separation points and different flow patterns is obviously observed. In CASE1 the symmetry stays normal, but in CASE2 the symmetry has lost because of the large flat area covered both upstream and downstream of the flow domain. In CASE3 and CASE4 5 < Re (=15 and 38) < 40 a firm pair of vortices appeared within the wake of the cylinder: whereas in CASE4 the fixed pair of vortices covered a larger area compare to CASE3).

İn CASE5 and CASE6 40 < Re (=160 and 190) < 200, the von Karman vortex street takes place. In CASE7 and CASE8 200<Re (= 250 and 290) <300, the wake of the elliptical cylinder is much turbulent than the circular cylinder. However, the square cylinder is much turbulent than the elliptical cylinder. As Reynolds number increased more 300<Re (10^3, 10^4, 10^5, $2.5*10^5$) <$3*10^5$ (CASE9 to CASE12) the wake behind the elliptical cylinder for CASE9 and CASE10 is completely turbulent, while CASE11 and CASE12 the wake become thinner and longer. When Reynolds number in increased Re>$3*10^5$, the wake at the back of the elliptical cylinder is thin and straight till the end of the downstream (CASE13 to CASE21).

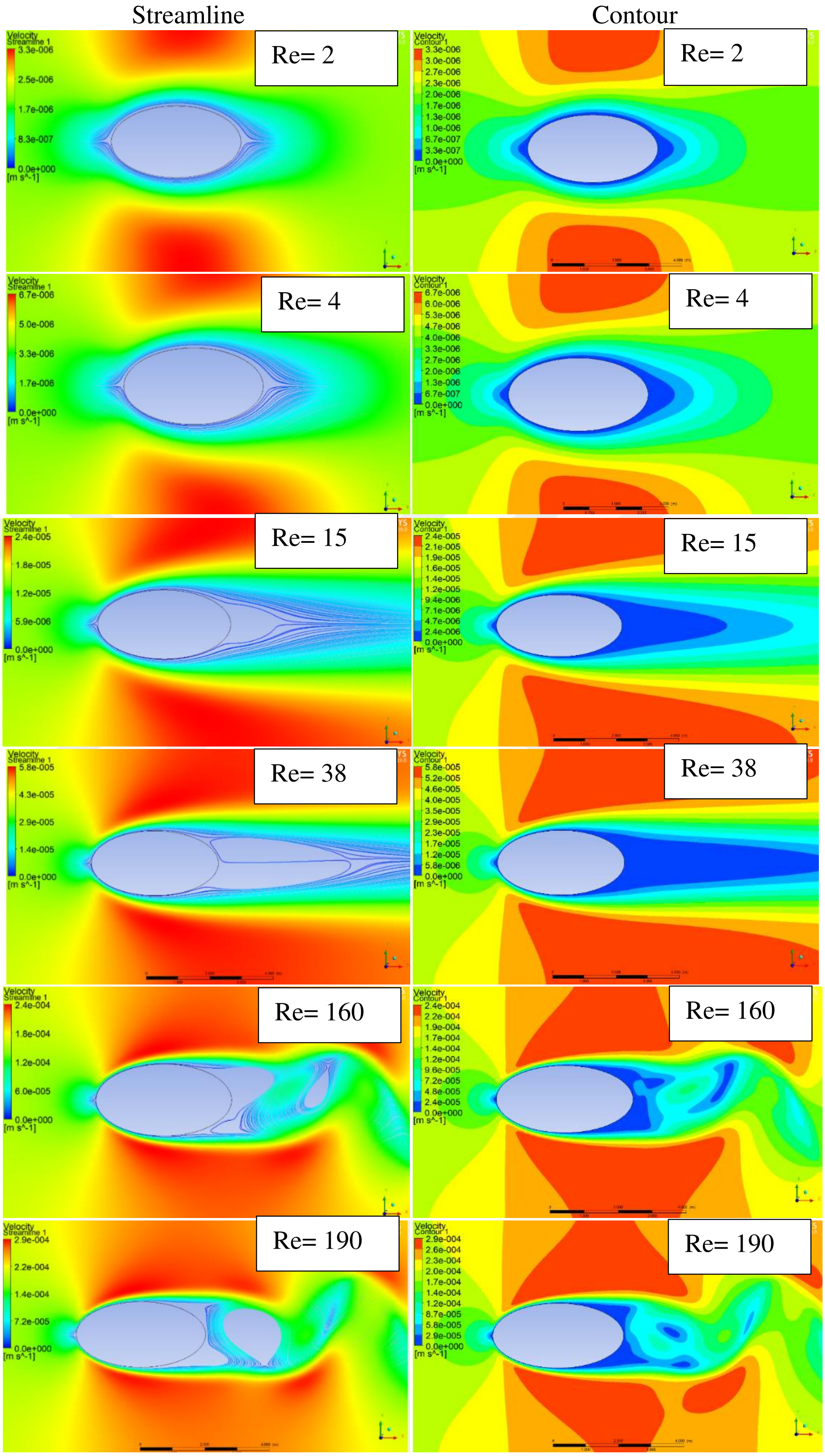

Figure 4.8 Flow around elliptic cylinder

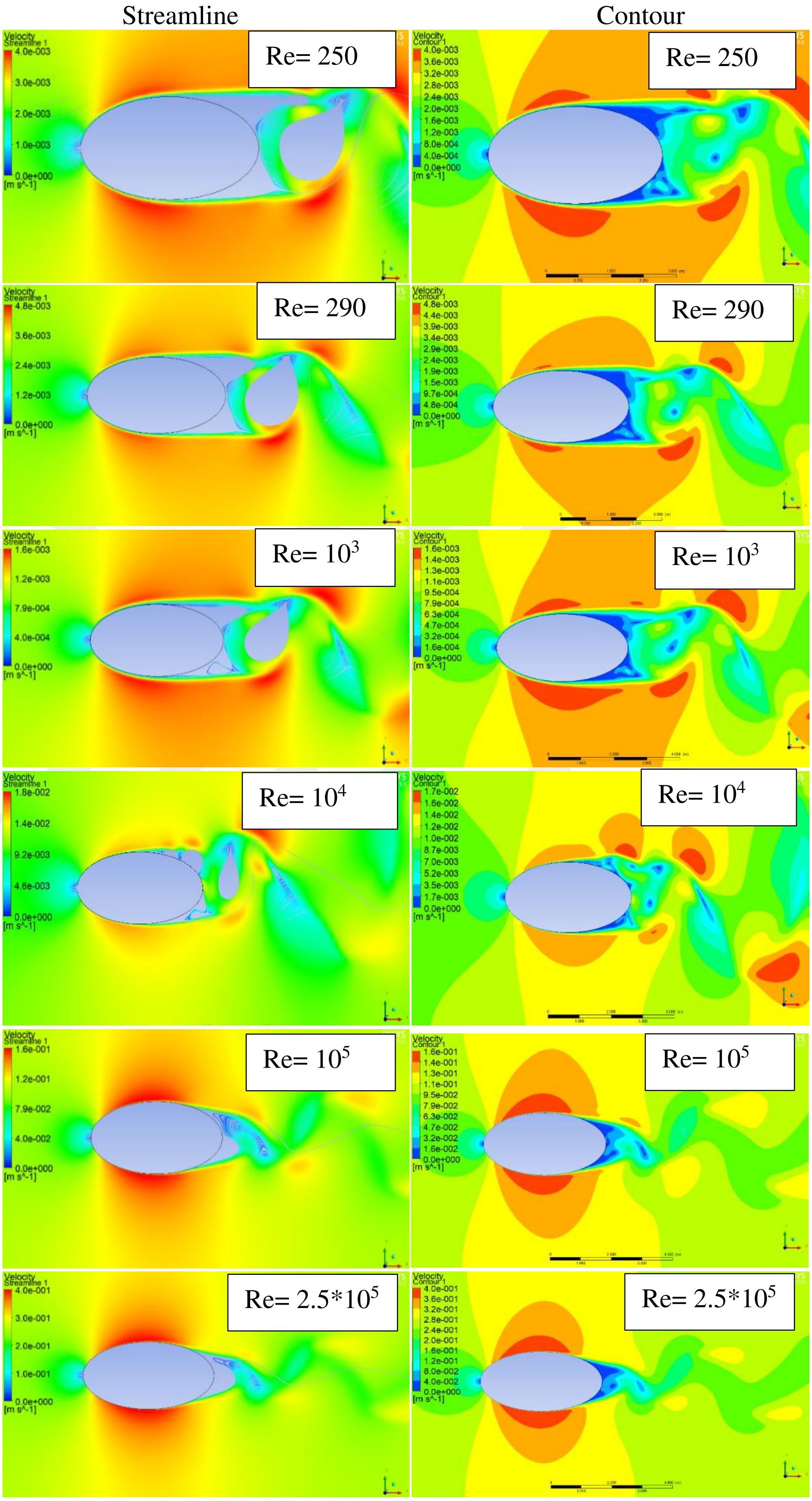

Figure 4.8 (cont.) Flow around elliptic cylinder

Streamline Contour

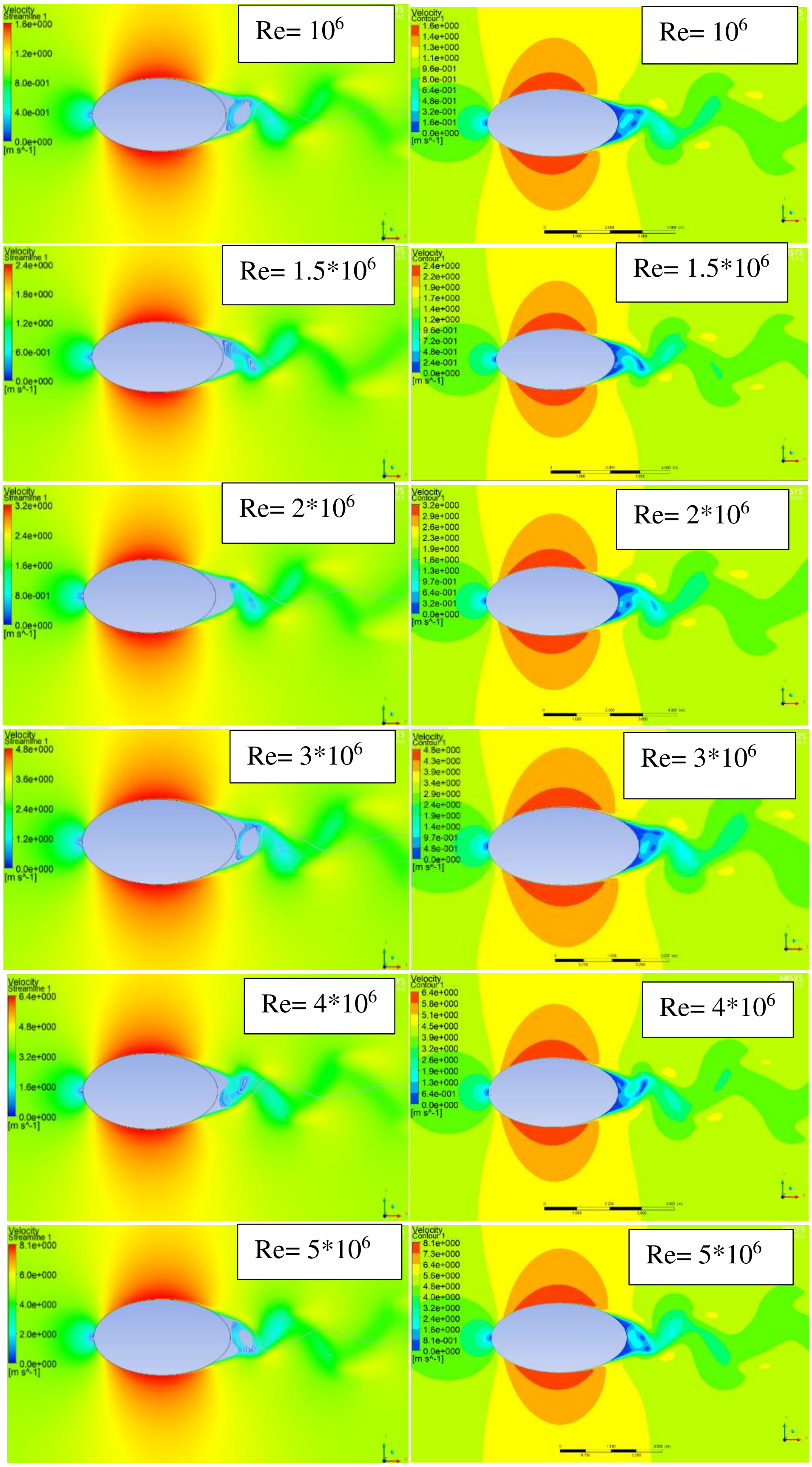

Figure 4.8 (cont.) Flow around elliptic cylinder

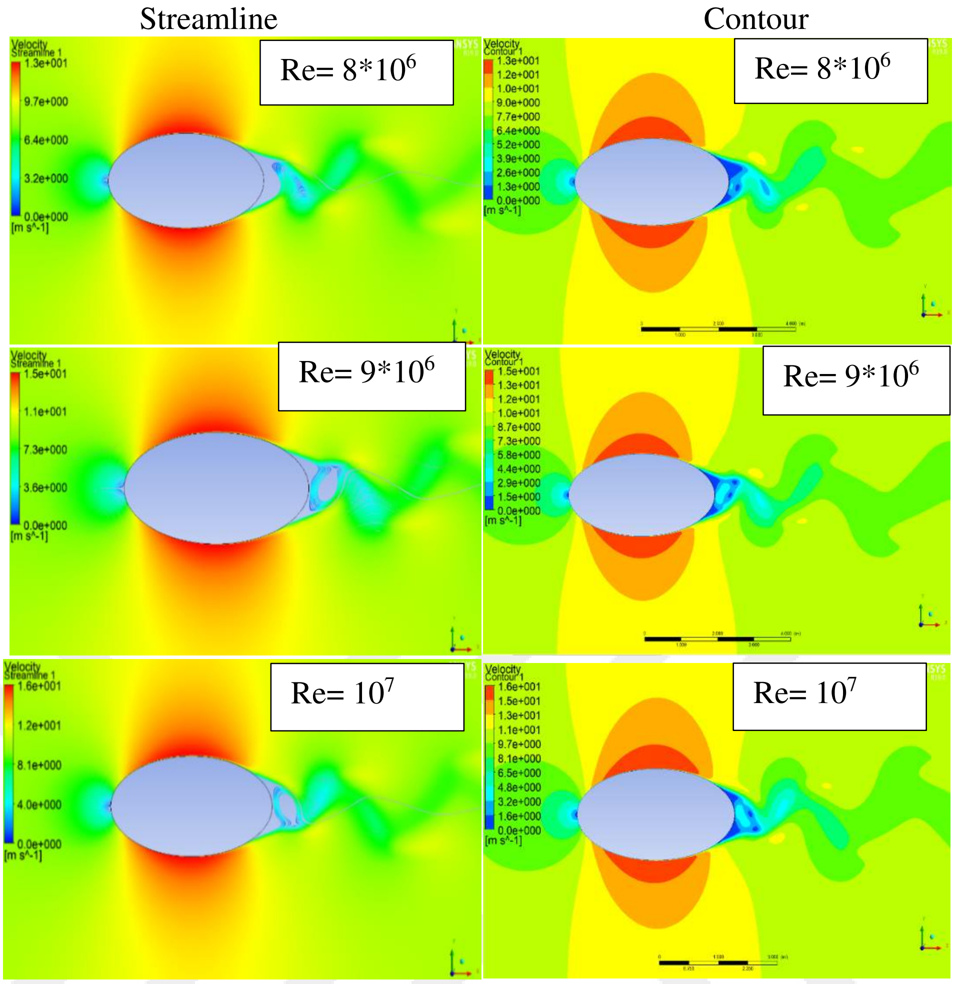

Figure 4.8 (cont.) Flow around elliptic cylinder

4.3.2 Velocity Profile

The velocity profiles of elliptical cylinder are taken different intervals compare to circular cylinder. These intervals are 2m, 3m, 4m, 6m, 9m, 12m and 15m at the upstream and 2m, 3.5m, 5m, 6m, 7m, 10m, 15m, 20m, 25m, 30m, 35m, 40m and 48m at the downstream. Because of The shape of the elliptical cylinder it has shown a small area of separated flow in the downstream compared to circular cylinder. In figure 4.9 it's going to illustrate the velocity profiles of flow around elliptical cylinders. CASE1 and CASE2 reveal the flow velocity change when flow reaches somewhere around and 2m downstream of the elliptical cylinder. As Reynolds number increase in CASE3 and CASE4 $5<Re<40$, a pair of left and right vortices is produced in the wake of the cylinder and the flow will be laminar. In CASE5 and CASE6 $40<Re<200$, Karman vortex street occurs and the flow becomes periodic. In CASE7 and CASE8 in elliptic cylinder the flow start transition from laminar to turbulent. From CASE9 to CASE21 the vortex street of elliptical cylinder is shorter and narrower than the circular cylinder.

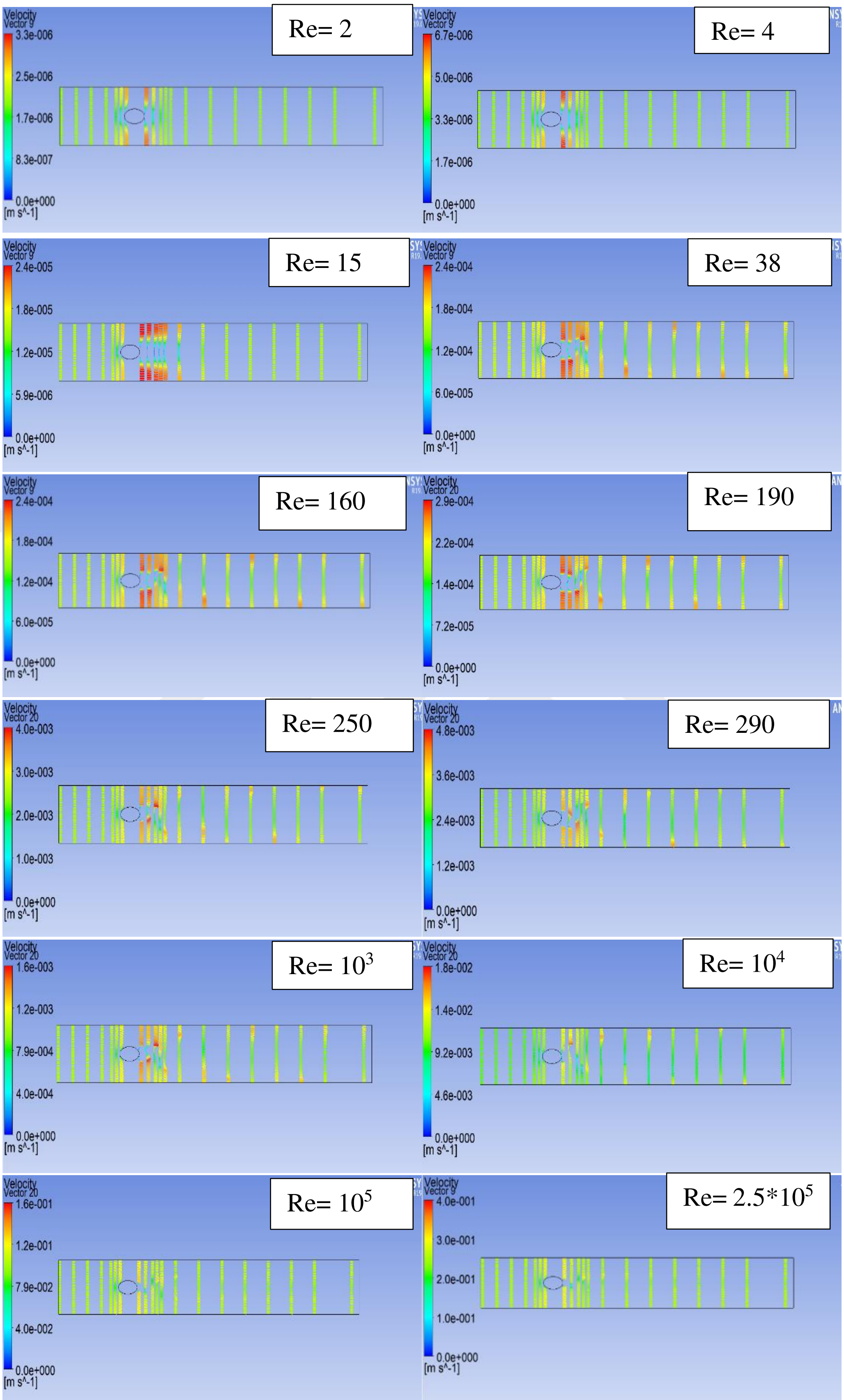

Figure 4.9 Velocity profile

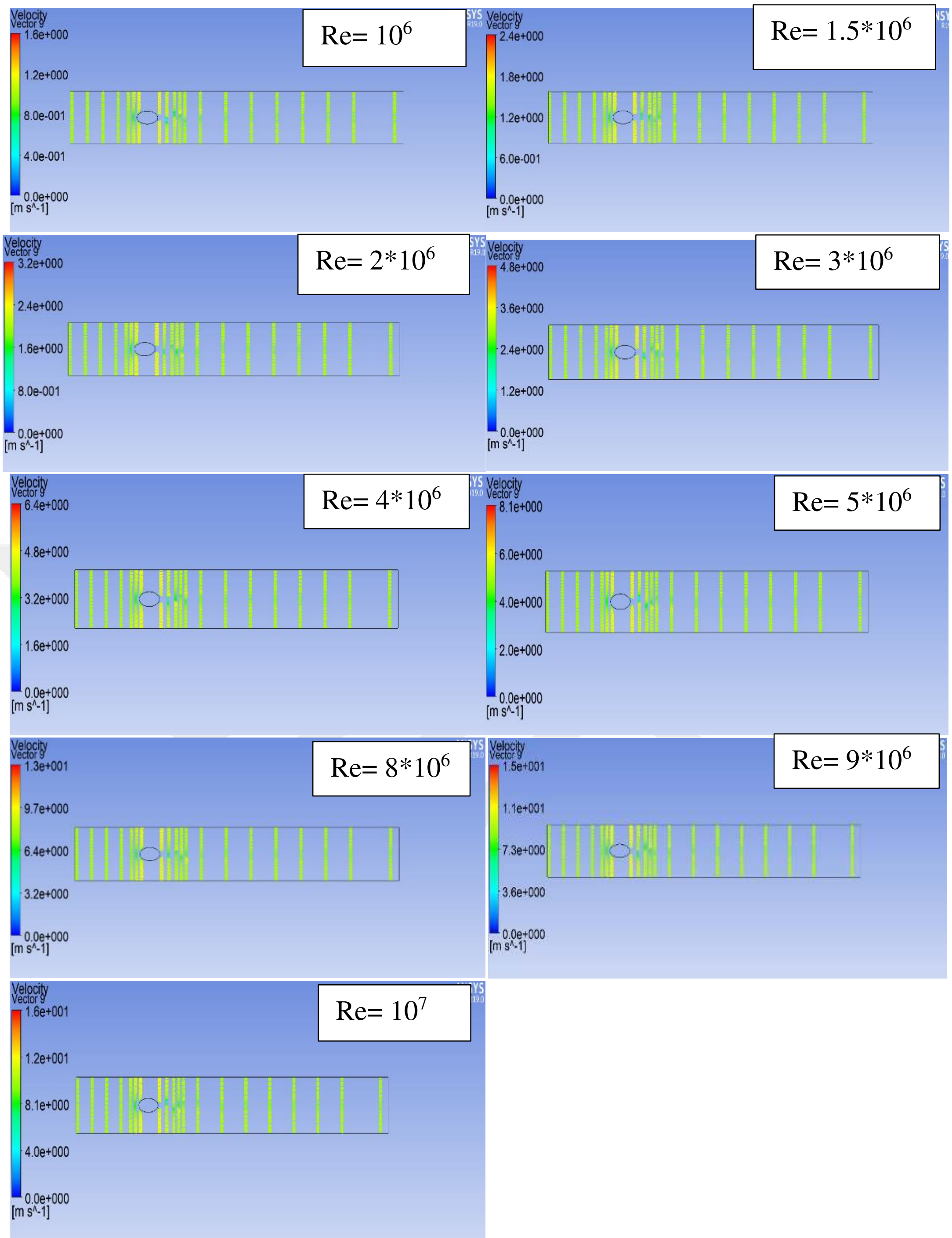

Figure 4.9 (cont.) Velocity profile

4.6 Comparison of Flow Around Circular, Elliptic and Square Cylinders

When the Reynolds number is 2, the circular and elliptical cylinder has symmetric streamlines from upstream to downstream of the flow domain and no flow separation took place. However, when it comes to the square cylinder various flow patterns and different flow separations is clearly observed. As Reynolds number expended to $5 < Re (=15 \text{ and } 38) < 40$ a fixed pair of vortices took place within the wake of the cylinders. As its shown in the figure 4.10 the vortices region of square cylinder is a little bit larger than the circular and elliptical cylinder. When the Reynolds number further increases to a range of $40<Re<200$, the von Karman vortex street takes place, in which vortex at first grows at one side of the cylinder and then detaches and grows again at other side. The angle of separation of square cylinder is greater than the circular and elliptic cylinder. When Reynolds number is increased to 10^3 and 10^5 ($300<Re<3*10^5$), the wake behind the circular became fully turbulent at range of the Reynolds number mentioned above. Furthermore, the wake for the elliptical cylinder became completely turbulent when Reynolds number is 10^3, whereas the wake of the elliptical cylinder became thin and straight at the Reynolds number of 10^5. This is because of the slenderness of the streamlined of the cylinder. However, the wake flow behind the square cylinder proves to be exceedingly chaotic. In figure 4.10 it is shown that flow conditions around cylinders for a certain Reynolds number.

Re = 2

Re = 15

Re = 38

Re = 160

Re = 10^3

Re = 10^5

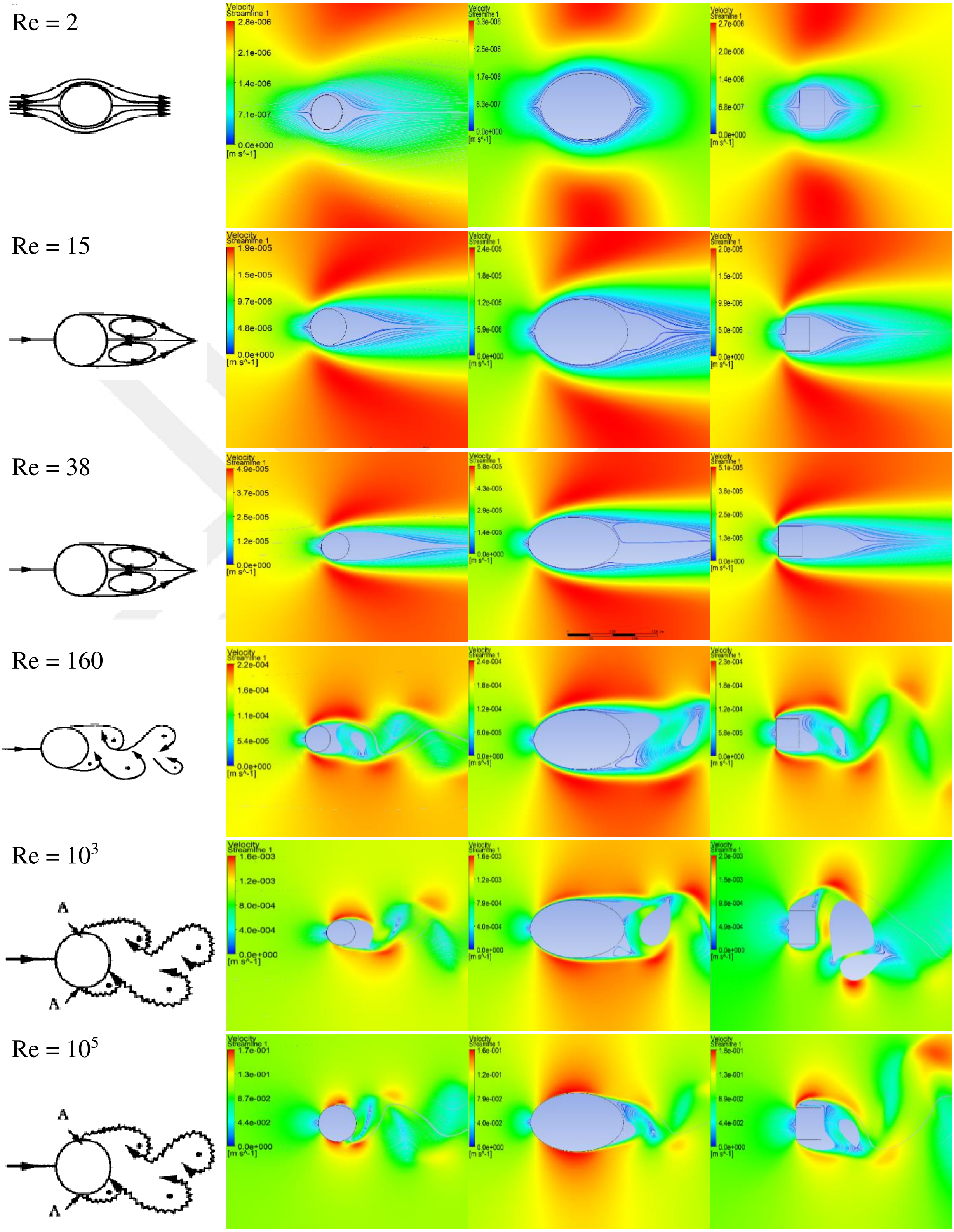

Figure 4.10 Flow conditions around cylinders for a certain Reynolds number

4.5 Drag Coefficient

The drag coefficient is a non-dimensional quantity which is used to describe the drag or the resistance of an obstacle in a fluid movement, such as water or air. The drag coefficient is designated as CD. The lower drag coefficient shows the object has less hydrodynamic or aerodynamic drag and vice versa. The drag coefficient is always related with a specific surface area, also it varies as a function of flow velocity, fluid density, fluid viscosity, flow direction, object size and so on. In this thesis, the drag coefficient of circular, square and elliptical cylinders at different Reynolds numbers were investigated by using CFD simulations. Shear stress transport (SST) k-w turbulence closure model were utilized in this simulation. Reynolds number of fluid flow around bluff body has direct impact on the value of the drag coefficient. Table 4.2 shows the values of the drag force and drag coefficient at various Reynolds number. The values of drag coefficient of square cylinder were obtained to be greater than the circular one.

Table 4.2 Drag force and drag coefficient on circular, elliptic and square cylinders at various Reynolds numbers

Re	**Total force on**			**Drag coefficients**				**Comparative difference with Hoener %**		
	Circular (N)	Elliptic (N)	Square (N)	Hoerner (1965)	Circular	Elliptic	Square	Circular	Elliptic	Square
2	$2*10^{-8}$	$3*10^{-8}$	$2.63*10^{-8}$	5.5	10	15	13.15	45	63.	58
4	$5*10^{-8}$	$7.52*10^{-8}$	$5.87*10^{-8}$	4	6.18	9.41	7.34	35	58	45
15	3.21*10	$4.97*10^{-7}$	$3.67*10^{-7}$	2.3	2.84	4.42	3.26	19	48	29
38	$1.34*10^{-6}$	$2.05*10^{-6}$	$1.54*10^{-6}$	1.65	1.85	2.84	2.13	10.81	42	22.5
160	$1.73*10^{-5}$	$2.32*10^{-5}$	$1.98*10^{-5}$	1.6	1.35	1.82	1.55	18.5	12	3
190	$2.40*10^{-5}$	$3.14*10^{-5}$	$2.87*10^{-5}$	1.5	1.32	1.74	1.59	12	13.8	6
250	0.0037	0.0040	0.0037	1.3	1.17	1.28	1.21	11	1.56	7
290	0.0047	0.0046	0.0012	1.1	1.12	1	2.84	1.71	10	61
10^3	0.00072	0.00065	0.0014	1	1.44	1.29	2.76	30.56	22.5	63.8
10^4	0.06	0.07	0.10	1.05	1.2	1.59	2.05	12.5	34	48.8
10^5	6.22	4.95	9.08	1.4	1.25	0.99	1.82	12	41	23
$2.5*10^5$	46.15	12.94	62.89	1.1	1.48	0.41	2.01	25.67	168	45
10^6	316	144.42	400.69	0.38	0.63	0.28	2.20	39.68	35.71	83
$1.5*10^6$	358	313.25	2154.93	0.5	0.68	0.27	1.91	26.47	85	74
$2*10^6$	752	556.38	4020.66	0.6	0.66	0.28	2.01	9	114	70
$3*10^6$	3008.93	1195.17	9675.88	0.7	0.67	0.26	2.15	4.47	169	67
$4*10^6$	5275.02	2115.39	15698.35	0.72	0.66	0.26	1.96	9	177	63
$5*10^6$	8406.03	3235.49	23687.45	0.75	0.67	0.26	1.89	12	188.46	60
$8*10^6$	19666	7737.23	64312.99	0.8	0.62	0.24	2.01	29	233	60
$9*10^6$	26412.4	9404.69	71747.95	0.85	0.65	0.23	1.77	30.76	270	52
10^7	30990	11192.1	101548.04	0.9	0.62	0.22	2.03	45.16	309	56

The outcomes of the experimental analysis which has done by Hoerner (1965) on a circular cylinder and the result of this analysis is shown in figure 4.11. The drag coefficient of circular, square and elliptic cylinders at low Reynolds number reduces linearly with the Reynolds number of these shapes. It's clear that the simulation results of the circular cylinder have well agreed to experimental results. However, the elliptic and square cylinders showed high difference compared with the experimental results. It has been observed that the shape of the cylinder has great effect on the value of drag coefficient. When Reynolds number is $10^3 < Re < 10^4$ the drag coefficient of elliptic cylinder is increased because of the difference in the conditions of wake flow. Due to the variation in the state of wake flow the drag coefficient of square cylinder rises when Reynolds number is $10^2 < Re < 10^4$. When Reynolds number is $10^5<Re<10^6$ the drag coefficient of circular cylinder increases quickly and then decreases. When Reynolds number increases further to $10^6<Re<10^7$ the drag coefficient of elliptic cylinder is reducing due to the slenderness of the streamlined cylinder. However, the circular cylinder has complied well with the experimental result in the range of these Reynolds number. This difference in the value of the drag coefficient is because of the separation point that is moving towards the downstream on the surface of the cylinder. İn figure 4.11 illustrated that the drag coefficient with respect to Reynolds number.

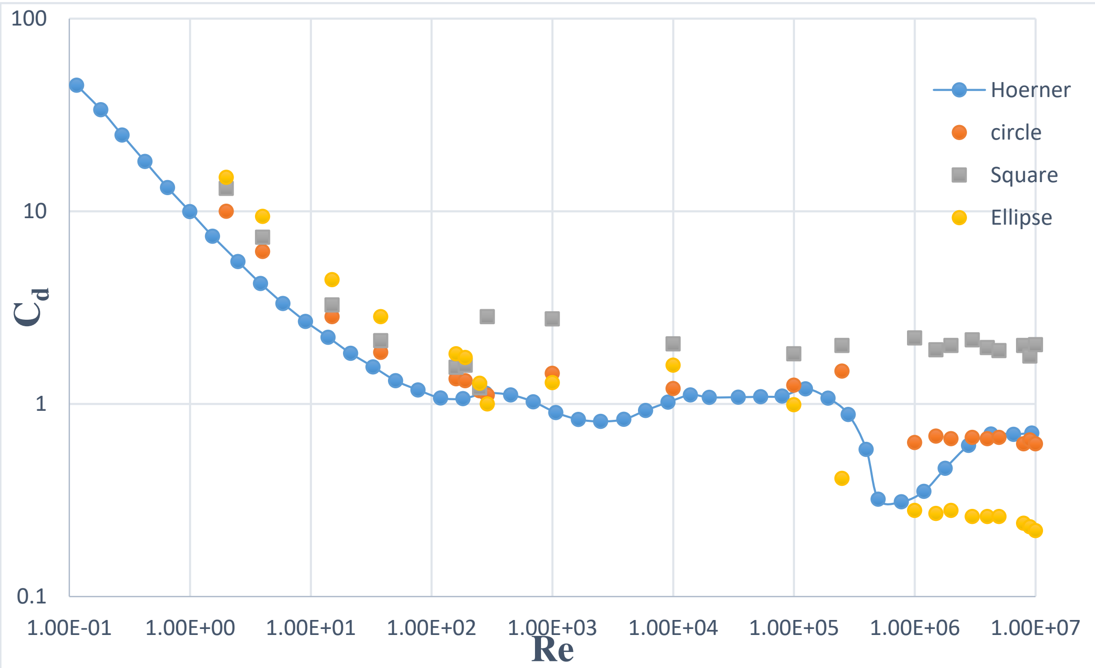

Figure 4.11 Drag coefficient with respect to Reynolds number

CHAPTER 5

CONCLUSIONS

Flow around circular, square and elliptic cylinders is considered in this study with Reynolds number ranging from 2 to $1*10^7$. Simulation investigations of the flow around cylinders were carried out by using Computational Fluid Dynamics (CFD). Flow domain and different drag coefficients of two-dimensional (2D) flow past vertical cylinders were investigated by utilizing FLUENT and shear stress transport (SST) k-ω turbulence closure model. Vertical cylinders might resemble bridge piers, offshore structures, tall buildings, etc. The magnitude of the Reynolds number and the shape of the cylinder have a great influence on both the vortex shedding and wake flow expanded behind the cylinders. It should be noted that the values of drag coefficient were obtained to be reducing with increase of Reynolds number. The drag coefficients acquired for the square cylinder were considered to be larger than the circular and elliptic ones under the same flow conditions. Wake flow behind the square cylinder was considerably broader than the circular and elliptic cylinders. The drag coefficient values for circular cylinder were noted to comply well with the experimental results carried out by the Hoerner (1965).

REFERENCES

Alrefaie, A. M. (2009). *Flow Control Around Circular Cylinder: Ventlation holes method.* Msc Thesis: University of Toledo.

Benim, A. C., Cagan, M., Nahavandi, A., Pasqualotto, E. (2007). RANS prediction of turbulent flow past a circular cylinder over the critical regime. *WSEAS International Conference on Fluid Mechanics and Aerodynamics* pp. 232-236. Athens.

Cao, S., Tamura, Y. (2009). Reynolds Number Dependence of the Velocity Shear Effects on Flow around Circular Cylinder. *EACWE 5* pp. 1-12. Florence: Tongji University.

Cao, Y., Tamura, T. (2016) Large-Eddy Simulations of Flow Past a Square Cylinder Using Structured and Unstructured Grids, *Computer and Fluids*, **137**, pp. 36-54.

Catalano, P., Wang, M., İaccarino, G., Moin, P. (2003). Numerical Simulation of Flow Around a Circular Cylinder at High Reynolds Number. *International Journal of Heat and Fluid*, **24**, pp. 463-469.

Cheng, M., White, D., Lou, J. (2007). Numerical Flow around a Square Cylinder in Uniform- Shear Flow. *Journal of Fluids and Structures*, **82**, pp. 207-226.

Didier, E. (2009). Numerical İnvestigations of Steady Flow Past an Elliptical Cylinder at Various Aspect Ratios. *Conference on Modelling Fluid Flow* pp. 1-8. Universidade Nova de press.

Hamielec, A. E., & Raal, J. (1969). Numerical Studies of Viscous Flow around Circular Cylinders. *Physics of Fluids*, **12**, pp. 1958-1988.

Hoerner, S. F. (1965). *Fluid Dynamic Drag, Practical İnformation on Aerodynamic Drag and Hydrodynamic Resistance.* New York City.

Islam, W. S., Raghavan, V. (2006). Numerical Simulation of High Sub-critical Reynolds Number Flow Past a Circular Cylinder. *Conference on Boundary and Interior Layers* pp. 1-8. University of Gottingen press.

Kareem, D. A. (2015). *A Numerical Analysis of Fluid Flow Around Circular and Square Cylinders.* Msc Thesis: Gaziantep university.

Kanaris, N., Grigoriadis, D., Kassinos, S. (2011). Three Dimensional Flow Around a Circular Cylinder Confined in a Plane Channel. *Physics of Fluids* , **23**, pp. 1-14.

Kim, M.-S., Sengupt, A. (2005). Unsteady Flow Over Elliptical Cylinders At Various Thickness with Different Reynolds Numbers. *Journal of Mechanical Science and Technology*, **19**, pp. 877-886.

Kumara, A., Raya, R. (2015). Numerical Study of Shear Flow Past a Square Cylinder at Reynolds Numbers 100, 200. *Procedia Engineering*, **127**, pp.102-109.

Mallick, M., Kumar, A. (2014). Study on Drag Coefficient for the Flow Past a Cylinder. *Internal Journal of Civil Engineering Research*, **5**, pp. 301-306.

Mehdi, H., Namdev, V., Kumar, P., Tyagi, A. (2016). Numerical Analaysis of Fluid Flow around a Circular Cylinder at Low Reynolds Number. *IOSR journal of mechanical and civil engineering*, **13**, pp. 94-101.

Menter, F. R. (1994). Two-Equation Eddy-Viscosity Turbulence Models for Engineering Applications. *AIAA Journal*, **32**, pp. 1598-1605.

Mostafa, M. S., Kamal, R., Gobran, M. (2014). Flow and Heat Transfer Characteristics Around and Elliptical Cylinder Placed İn Front of a Curved Plate. *Journal of Thermal Science*, **18**, pp 465-478.

Nair, M. T., Sengupta, T. (1997). Unsteady Flow Past a Circular Cylinder. *Journal of Fluids and Structures*, **11**, pp 555-595.

Noor, N. B. (2015). *Analysis of Vortex Shedding in a Various Body Shapes.* Msc Thesis: University Tun Hussein Onn Malaysia.

Okajima, A., Nagahisa, T., Akira, R. (1990). A Numerical Analysis of Flow around Rectangular Cylinders. *JSME international journal. Ser. 2, Fluids engineering, heat transfer, power, combustion, thermophysical properties*, **33,** pp. 702-711.

Ong, M. C., Utnes, T., Holmedal, L., Myrhaug, D., Pettersen, B. (2010). Numerical Simulation of Flow Around Circular Cylinder Close to a Flat Seabed at High Reynolds Number Using a k-ε Model. *Coastal Engineering*, **57**, pp 931-947.

Ong, M. C., Utnes, T., Holmedal, L., Myrhaug, D., Pettersen, B. (2009). Numerical Simulation of Flow around a Smooth Circular Cylinder at Very High Reynolds Numbers. *Marine Structures*, **22**, pp 142-153.

Rajani, B. N., Kandasamy, A., Majumdar, S. (2012). On The Reliability of Eddy Viscosity Based Turbulence Models Predicting Turbulent Floe Past a Circular Cylinder Using RANS Approach. *Journal of Applied Fluid Mechanics*, **5**, pp 67-79.

Rawat, M., Gupta, R., Sarviya, R. (2013). Numerical Simulations of Flow around an Elliptical Cylinder at High Reynolds Numbers. *İnternational Journal of Fluids Engineering*, **5**, pp 29-37.

Sharma, A., Eswaran, V. (2004). Heat and Fluid Flow across a Square Cylinder in the Two-Dimensional Laminar Flow Regime. *Numerical Heat Transfer*, **45**, pp 247-269.

Summer, B. M., Fredsoe, J. (1997). *Hydrodynamics Around Cylindrical Structures, Advanced Series on Ocean Engineering,* **12**, World Scientific Publishing Co. Pre. Ltd, Singapor.

Taeibi-Rahni, M., Esfahanian, V., Salari, M. (2013). Investigations of Flow Around a Confined Elliptical Cylinder Using the Lattice Boltzmann. *Middle-East Journal of Scientific Research*, **15**, pp 08-13.

Wilcox, D. C. (1998). *Turbulence Modelling for CFD.* DCW Industries, Inc., a La Canada.

Yen, C, S., Yang, C. (2011). Flow Patterns and Vortex Shedding Behavior Behind a Square Cylinder. *Journal of wind engineering and industerial aerodynamics*, **99**, pp 868-878.

Yuce, M. I., Kareem, D. (2016). A Numerical Analysis of Fluid Flow around Circular and Square Cylinders. *American Water Works Association*, **108**, pp 546-554.

Zhang, X.-T., Li, Z.-Y., Fu, S.-X., Ong, M., Chen, Y. (2014). Study of Flow around the Cylinder from Subcritical to Supercritical Regimes. *Ocean System Engineering*, **4**, pp 1-17.

Zhao, M., Lu, L. (2018). Numerical Simulations of Flow Past Circular Cylinders in Cruciform Arrangment. *Journal of fluid Mech*, **848**, pp 1013-1039.